Zhou et al. *Zool. Res.* 2025, 46(3): 551−575
https://doi.org/10.24272/j.issn.2095-8137.2024.445
https://cstr.cn/32248.14.zr.2024.445

ZR | Zoological Research

Review Open Access

Large animal models for investigating the applications of photodynamic therapy

Heng-Zong Zhou[1,#], Dong-Xu Wang[1,2,#], Yu-Qiang Qian[1], Jia-Qi Wei[1], Sen Ma[3], Yu-Jing Feng[1], Yang Hao[1,2,*]

[1] *Department of Laboratory Animals*, *College of Animal Sciences*, *Jilin University*, *Changchun*, *Jilin* 130062, *China*

[2] *Zhichuang Gene Editing Animal Model Research Center*, *Wenzhou Institute of Technology*, *Wenzhou*, *Zhejiang* 325000, *China*

[3] *Department of Ophthalmology*, *Leiden University Medical Centre (LUMC)*, *Leiden*, *Zuid-Holland* 2333 *ZA*, *The Netherlands*

ABSTRACT

Photodynamic therapy (PDT) is an emerging minimally invasive therapeutic modality that relies on the activation of a photosensitizing agent by light of a specific wavelength in the presence of molecular oxygen, leading to the generation of reactive oxygen species (ROS). This mechanism facilitates selective cytotoxic effects within pathological tissues and has demonstrated therapeutic potential across diverse disease contexts. However, the broader clinical applications remain limited by photosensitizer selectivity, shallow light penetration, and the risk of off-target cytotoxicity. Recent advancements in PDT have focused on the development of next-generation photosensitizers, the integration of nanotechnology for enhanced delivery and targeting, and the strategic combination of PDT with complementary therapeutic approaches. Experimental animal models play a crucial role in validating the efficacy and safety of PDT, optimizing its therapeutic parameters, and determining its mechanisms of action. This review provides a comprehensive overview of PDT applications in various disease models, including oncological, infectious, and nonconventional indications. Special emphasis is placed on the importance of large animal models in PDT research, such as rabbits, pigs, dogs, and non-human primates, which provide experimental platforms that more closely resemble human physiological and pathological states. The use of these models for understanding the mechanisms of PDT, optimizing therapeutic regimens, and evaluating clinical outcomes is also discussed. This review aims to inform future directions in PDT research and emphasizes the importance of selecting appropriate preclinical animal models to facilitate successful clinical translation.

Keywords: Photodynamic therapy; Cancer; Infection; Animal models

INTRODUCTION

Photodynamic therapy (PDT), initially developed by Danish physician Niels Finsen for the treatment of lupus vulgaris, has evolved into a versatile and minimally invasive therapeutic strategy with expanding clinical applications (Daniell & Hill, 1991). Its primary advantage lies in its capacity to induce localized cytotoxicity in pathological tissues while protecting adjacent healthy structures. This selectivity underpins its utility across multiple disciplines, including oncology, ophthalmology, cardiology, dermatology, and the treatment of atherosclerosis (Hao et al., 2022b). PDT involves the systemic or local administration of a photosensitizer (PS), which preferentially accumulates in pathological tissues. Upon exposure to light of a specific wavelength (hv), the PS transitions from its ground singlet state to an excited singlet state. The PS in its excited singlet state can dissipate energy either by emitting a photon as fluorescence or by undergoing internal conversion to a more stable, long-lived triplet state, which induces localized photochemical reactions in the presence of molecular oxygen. Type I photochemical pathways produce free radicals such as superoxide anion radical ($O_2^{-\bullet}$), hydroxyl radical ($OH\bullet$), and hydrogen peroxide (H_2O_2), while type II pathways generate singlet oxygen ($^1O_2$). These reactive oxygen species (ROS) damage intracellular macromolecules, including proteins, lipids, and nucleic acids, ultimately leading to cell death (Kwiatkowski et al., 2018). Beyond direct cytotoxicity, PDT also exerts anticancer effects by disrupting tumor vasculature and stimulating antitumor immune responses, contributing to its therapeutic efficacy (Castano et al., 2006) (Figure 1).

Animal models are indispensable in advancing PDT from preclinical research to clinical application (Silva et al., 2015).

Received: 18 February 2025; Accepted: 12 March 2025; Online: 13 March 2025

Foundation items: This work was supported by the China Postdoctoral Science Foundation (2024M751098, 2024M761134), Jilin Province Development and Reform Commission Program (ZKJCFGW2023015), Wenzhou Science & Technology Bureau Basic Public Welfare Research Program (Y20240006), and Jilin University Young Teachers and Students Cross-disciplinary Training Project (2023-JCXK-08)

[#]Authors contributed equally to this work

*Corresponding author, E-mail: yhao@jlu.edu.cn

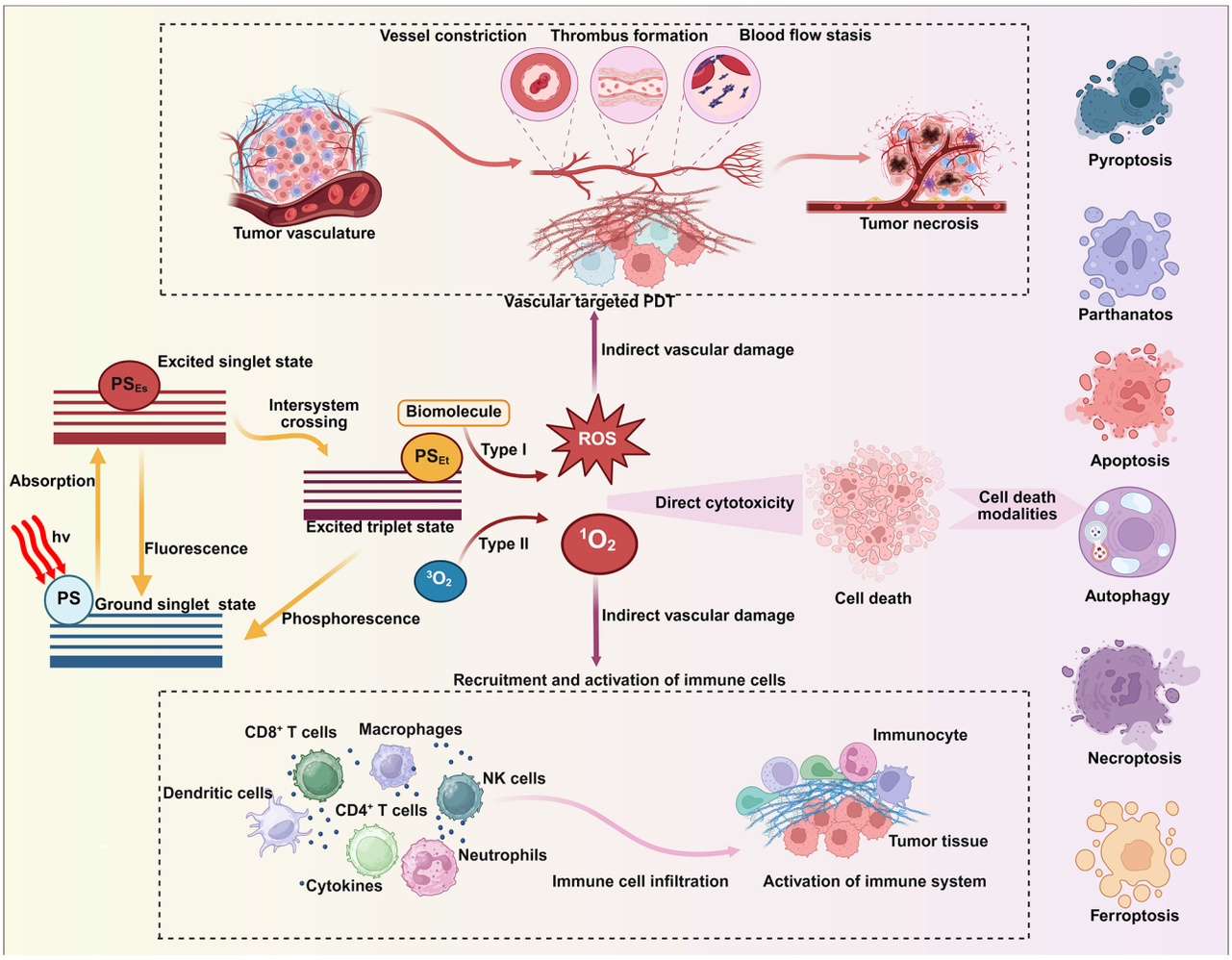

Figure 1 Schematic of photodynamic therapy (PDT) mechanism in cancer cells

In cancer treatment, the PDT mechanism involves administration of a photosensitizer (PS), which accumulates in tumor cells. Upon exposure to specific-wavelength light, the PS generates reactive oxygen species (ROS) and singlet oxygen ($^1O_2$) to induce tumor cell death and damage tumor vasculature, leading to ischemic cell death. PDT also triggers inflammation and immune responses against tumor progression. Figure created with Bioender.com.

Small animal models, particularly mice and rats, are widely used in PDT studies due to their low cost, genetic manipulability, and ease of handling (Silva et al., 2015). However, the substantial genetic, physiological, and anatomical disparities between humans and small animals may markedly impact disease manifestation and treatment response (Bonnotte et al., 2003; Maas et al., 2012). In addition, the small size of mice poses challenges for procedures involving complex imaging, surgical intervention, or repeated sampling (Kessels et al., 2018). These limitations have prompted a shift toward larger animal models that offer greater anatomical and physiological resemblance to humans (Ziegler et al., 2016). Species such as rabbits, pigs, dogs, sheep, and non-human primates (NHPs) provide a more physiologically relevant platform for assessing the efficacy and safety of PDT regimens (Ziegler et al., 2016), as well as pharmacokinetics, biodistribution, light penetration dynamics, and tissue responses. Their use enables the refinement of light dosimetry, photosensitizer delivery strategies, and treatment protocols under clinically relevant conditions.

This review explores the strategic use of animal models in PDT research, emphasizing the importance of appropriate model selection for assessing the therapeutic effects and mechanisms of PDT for specific disease indications. Particular focus is given to large animal models and other emerging preclinical platforms, evaluating their advantages and disadvantages. By highlighting the contributions of these models to mechanistic insight, therapeutic optimization, and efficacy assessment, this review aims to inform future directions in PDT development and preclinical validation.

PHOTOSENSITIZERS

Development of photosensitizers

The therapeutic efficacy of PDT is governed by the selective accumulation and retention of PS within diseased tissues, availability of sufficient oxygen, and irradiation of light at an appropriate wavelength (Castano et al., 2006). The choice of PS is therefore central to treatment outcomes and should exhibit high selectivity for pathological tissues and strong absorption at the wavelengths within the 600–800 nm range. This band of light, commonly referred to as the therapeutic window, allows for deeper tissue penetration while avoiding the absorption peaks of endogenous chromophores such as hemoglobin and cytochromes (Yoon et al., 2013). Many different types of PS molecules have been developed to meet

these criteria.

First-generation PS, typified by hematoporphyrin derivatives (HpD) and porfimer sodium (Photofrin®), were instrumental in establishing PDT as a clinical modality (Furuse et al., 1993). However, these agents have several drawbacks, including suboptimal absorption characteristics, limited tissue selectivity, prolonged skin photosensitivity, and localized pain (O'Connor et al., 2009). To address these limitations, second- and third-generation PS have been developed with improved photophysical and pharmacokinetic profiles. Second-generation PS are predominantly based on porphyrin or chlorin structures but exhibit enhanced purity, solubility, and tissue targeting. Representative compounds include 5-aminolaevulinic acid (5-ALA), meta-tetrahydroxyphenylchlorin (mTHPC, FOSCAN®), and benzoporphyrin derivative monoacid ring A (BPD-MA, Verteporfin®). Notably, 5-ALA serves as a prodrug that can be enzymatically converted to protoporphyrin IX (PpIX) within cells via the heme biosynthesis pathway, leading to ROS generation upon light activation. These PS have maximum absorption wavelengths within the 630–700 nm range, offering improved activation efficiency and deeper tissue penetration compared to earlier agents (Kwiatkowski et al., 2018). Third-generation PS include those engineered for tumor-specific targeting and are still under development. In recent years, nanoparticles (NPs) (1–100 nm) have emerged as a promising approach due to their enhanced permeability and retention (EPR) and subcellular size (Joudeh & Linke, 2022; Khan et al., 2019). Additionally, NPs support deeper tissue penetration and more efficient accumulation of PS, thereby enhancing PDT efficacy (Lucky et al., 2015). Beyond passive targeting, photoresponsive NPs, such as metallic ZnO and Au NPs, as well as upconversion nanoparticles (UCNPs), can absorb long-wavelength near-infrared (NIR) light and emit specific short-wavelength UV or visible light for deeper penetration (Ansari et al., 2022, 2024). Multifunctional NPs can also be surface-modified with targeting moieties, such as ligands, monoclonal antibodies, and peptides, or combined with complementary imaging or therapeutic platforms, including photoacoustic imaging and photothermal therapy, to enhance treatment precision and real-time monitoring (Wang et al., 2021; Mauro et al., 2021). These advanced PS systems offer improved targeting and bioavailability and are expected to drive significant breakthroughs in PDT-based cancer therapy (Wang et al., 2021).

Despite these advancements, challenges remain in ensuring the long-term safety, stability and scalable production of next-generation PS. Future research must also address the development of efficient light delivery systems, including external, portable, or implantable sources, to achieve uniform light distribution and adequate activation within target tissues (Li & Lin, 2022; Piksa et al., 2023). Additionally, artificial intelligence presents a promising avenue for predicting the photophysical properties and biodistribution of novel PS compounds, thereby accelerating their rational design and clinical translation.

Lipoprotein profiles in animal models for PS delivery

Lipoproteins serve as essential carriers for hydrophobic lipids in circulation, forming dynamic complexes with lipids and apolipoproteins, which stabilize particle structure and mediate cellular uptake via receptor interactions. These particles are classified based on size and density into very low-density lipoproteins (VLDLs), intermediate-density lipoproteins (IDLs; VLDL remnants), low-density lipoproteins (LDLs), and high-density lipoproteins (HDLs) (Wasan & Cassidy, 1998). The hydrophobic nature of PS facilitates their preferential association with circulating lipoproteins, with LDL and HDL fractions playing critical roles in determining biodistribution and tumor targeting efficiency (Huang et al., 2015). LDL particles, typically 18–25 nm in diameter and rich in cholesteryl esters, present apolipoprotein B-100 (ApoB-100) on their surface, which is specifically recognized by the LDL receptor (LDLR) (Goldstein & Brown, 2009; Olofsson & Borèn, 2005; Segrest et al., 2001). Rapidly proliferating tumor cells often exhibit up-regulated expression of LDLRs (e.g., lectin-like oxLDL-1 (LOX-1) and oxidized LDL receptor OLR1), resulting in preferential enrichment of LDL-bound PS in tumor tissue (Hirsch et al., 2010; Ma et al., 2019; Nakashima-Nakasuga et al., 2020). For example, approximately 80% of BPD-MA in human plasma is associated with LDL, and its uptake via LDLR-mediated endocytosis significantly enhances PDT efficacy in tumor tissue (Allison et al., 1991, 1994). Encapsulation of PS within the lipophilic core of LDL particles or synthetic lipid-based NPs also improves tumor targeting and reduces off-target toxicity without compromising the physicochemical properties of the therapeutic agent (Konan et al., 2002).

However, substantial interspecies variation in lipoprotein profiles presents a challenge for translational PDT research. In mice, HDL particles (8–12 nm) constitute approximately 60%–80% of total plasma cholesterol, whereas LDL accounts for only 5%–10%. Rats exhibit a similar pattern, with HDL comprising 50%–60% of total cholesterol —still markedly higher than in humans (25%–35% for HDL and 60%–70% for LDL) (Yin et al., 2012). These discrepancies arise in part from the absence of cholesteryl ester transfer protein (CETP) in rodent plasma, a key regulator of cholesterol metabolism in humans (Kurano et al., 2017). As a result, PS in rodents bind preferentially to HDL, which undergoes hepatic clearance via hepatic scavenger receptor B1 (SR-B1), reducing plasma half-life and tumor accumulation of HDL-bound PS such as HpD (Kessel, 1986; Marques et al., 2019). Despite the limitations of lipoprotein profiles and depth of light penetration, rodent models, especially genetically engineered mice, remain indispensable for mechanistic investigations of PDT. For example, CETP-transgenic mice that exhibit a more human-like LDL/HDL ratio (with LDL increased to 40%–50%) provide a more accurate pharmacokinetic profile for LDL-bound PS (Dinchuk et al., 1995). Additionally, strategies such as intratumoral injection or the use of nanocarrier-encapsulated PS allow circumvention of systemic lipoprotein metabolism, enabling localized PS accumulation and improved therapeutic outcomes (Fan et al., 2023).

In summary, interspecies differences in lipoprotein composition significantly influence the pharmacokinetics and tumor-targeting behavior of PS. Understanding and accounting for these variations is critical for selecting appropriate animal models and optimizing PDT protocols. Subsequent sections will examine the lipoprotein characteristics of various animal models and their implications for preclinical PDT research.

RABBIT MODELS IN PDT RESEARCH

Rabbits, members of the order Lagomorpha and family Leporidae, include more than 100 recognized species and

strains. Among these, several breeds, including Polish, Dutch-belted, New Zealand White, Japanese White, and Chinese White rabbits, are commonly used in biomedical research (Sengupta & Dutta, 2020). Owing to their intermediate size, rabbits serve as an effective translational model bridging small rodent studies and large animal preclinical validation in PDT. Their anatomical and physiological features, particularly in ocular and vascular systems, closely resemble those of humans, making them especially suitable for studying PDT applications in age-related macular degeneration (AMD), choroidal neovascularization (CNV), and other ophthalmic disorders (Peiffer et al., 1994). In addition to ophthalmology, rabbit models are extensively employed in cardiovascular research, oncology, dermatology, and infectious disease modeling due to their moderate body size, accessible vasculature, appropriate skin thickness, and low maintenance costs (Figure 2).

Rabbit models for ophthalmological research of PDT

Rabbits represent a highly suitable preclinical model for evaluating the efficacy of PDT in ophthalmic diseases due to their accessible ocular anatomy, procedural compatibility, and significant physiological similarities to the human eye. Early investigations in the 1980s employed iris xenografts in melanoma-free pigmented rabbits to explore the ocular distribution and photodynamic effects of HpD, a first-generation PS. Following systemic administration, HpD was found to accumulate in intraocular tumors, vascular structures such as the iris and choroidal retina, and atrial fluid of affected eyes. Irradiation produced significant tumor-localized effects without overt ocular toxicity, indicating the potential of HpD-PDT in treating intraocular malignancies (Gomer et al., 1985). However, HpD exhibited prolonged retention in normal tissues (e.g., skin), resulting in systemic phototoxicity, slow metabolic clearance, and increased risk of unintended tissue damage post-treatment, limiting its clinical utility. To overcome these limitations, various second-generation PS have been developed and evaluated in rabbit models, particularly for ocular diseases characterized by aberrant neovascularization, such as AMD, CNV, and diabetic retinopathy (Holzer et al., 2003; Sawa et al., 2004; Tsilimbaris et al., 1994; Wilson et al., 1991). Among these, BPD-MA (Verteporfin®) demonstrates favorable pharmacokinetics, including rapid clearance from healthy tissues and activation at 689 nm, enabling deeper tissue penetration with reduced systemic toxicity. Prior to clinical approval for AMD, several Verteporfin®-based PDT protocols were systematically validated in rabbits, using both healthy models and those with experimentally induced CNV (e.g., intrastromal filament placement or intracorneal suturing near the limbus). In a representative study, Lin et al. (1994) conducted fluorescein angiography and fundus photography in Dutch-belted rabbits prior to PDT. Notably, Verteporfin® was administered intravenously at 1 mg/kg via the marginal ear vein, followed by laser irradiation at 688 nm with a fluence rate of 314 mW/cm^2. This procedure successfully induced choroidal vessel occlusion without causing acute thermal injury. Histological evaluation revealed damage to choroidal

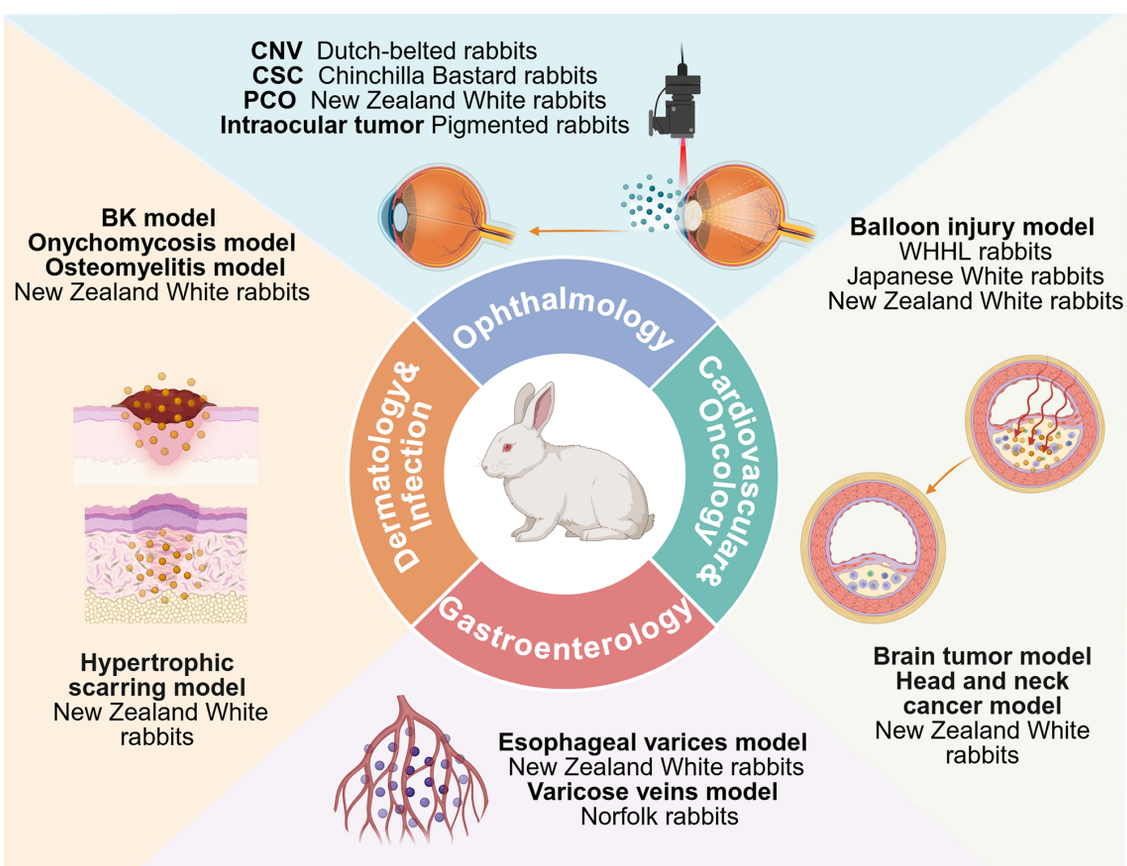

Figure 2 PDT applications in rabbits for different pathological conditions, including cancer, bacterial infections, and neoplastic conditions, highlighting specific disease models

CSC: Central serous chorioretinopathy; CNV: Choroidal neovascularization; PCO: Posterior capsular opacification; WHHL: Watanabe hereditary hyperlipidemia; BK: Bacterial keratitis. Figure created with BioRender.com.

vascular endothelial cells, retinal pigment epithelium (RPE), neural retina and Bruch's membrane (Lin et al., 1994). The study also noted subtle differences in PDT-induced damage between pigmented and non-pigmented (albino) rabbits, attributed to fundus pigmentation, which may reflect light from the sclera and alter intraocular light distribution at lower energy densities—though this effect is considered minimal in clinical practice (Peyman et al., 2000). Comparative studies have also assessed the efficacy and safety of novel PS. For example, Berdugo et al. (2008) demonstrated that WST-11 (TOOKAD®), when applied at a fluence of 50 J/cm^2, drug dose of 5 mg/kg, and drug-light interval (DLI) of 1 min, effectively occluded abnormal choroidal vessels while causing less damage to RPE and retinal structures compared to Verteporfin®-PDT. Other PS, such as Rose Bengal, chloroaluminum-sulfonated phthalocyanine (CASPc), dihydroporphyrin e6, and ATX-S10 (Na), showed preferential accumulation in the choroid and RPE of rabbit eyes, although biodistribution patterns varied among compounds (Gohto et al., 2000; Haimovici et al., 2002)

Despite encouraging preclinical results, many PS-mediated PDTs and combination therapies have not progressed to clinical approval (Table 1). Optimization of light parameters —including wavelength, fluence, and exposure duration—remains essential to maximize efficacy and reduce retinal damage in rabbit models (Chuang et al., 2014). The clinically established protocol for treating human neovascular AMD involves intravenous Verteporfin® infusion over 15 min, followed by laser irradiation at 689 nm for 83 s at a fluence rate of 600 mW/cm^2 (total fluence: 50 J/cm^2). This regimen is particularly effective for treating classic CNV lesions, resulting in reduced hemorrhage, decreased exudation, and stabilization of vision. In addition, combining rabbit anti-mouse vascular endothelial growth factor (VEGF) polyclonal antibodies with Verteporfin® has shown promise in rabbit studies, suggesting a viable approach for synergistic treatment

Table 1 Rabbits used for PDT research

Disease	Specialty	Animal	PDT regimen	References
Central serous chorioretinopathy (CSC)	Ophthalmology	Chinchilla Bastard rabbits	Verteporfin®, DLI 15 min, 689 nm, 50 J/cm^2, 600 W/cm^2, 83 s	Du et al., 2021
Posterior capsule opacification (PCO)	Ophthalmology	New Zealand White rabbits	RB, DLI after surgery, visible light 420–500 nm; 160 J/cm^2, 500 mW/cm^2, 2 min	Koh et al., 2002
CNV	Ophthalmology	Dutch-belted rabbits	Verteporfin®, DLI immediately, 688 nm, 314 mW/cm^2, 1 min	Lin et al., 1994
CNV	Ophthalmology	Dutch-belted rabbits	Verteporfin®, DLI immediately, 689 nm, 17 J/cm^2 or 50 J/cm^2 or 150 J/cm^2, 600 mW/cm^2	Holzer et al., 2003
CNV	Ophthalmology	Pigmented rabbits (Strain: Not mentioned)	ICG, DLI 10s, 753 nm, 2.3–28.5 J/cm^2, 230 or 630 or 950 mW/cm^2	Costa et al., 2001
CNV	Ophthalmology	Dutch-belted rabbits	PhotoPoint MV6401 (indium chloride methyl pyropheophorbide), DLI 10–60 min, 664 nm, 5–25 J/cm^2, 150 mW/cm^2	Ciulla et al., 2005
CNV	Ophthalmology	Chinchilla Bastard rabbits	WST09, DLI 5–60min, 650 nm, 3–200 J/cm^2, 600 mW/cm^2 for total fluence of 1.89 mW ± 10%	Framme et al., 2006b
CNV	Ophthalmology	Chinchilla Bastard rabbits	Verteporfin®, DLI 15min, 689 nm, 600 mW/cm^2, 83s	Du et al., 2021
CNV	Ophthalmology	Pigmented Californian rabbits	Chlorophyllin-M (chlorophyll-based derivative), 660 nm, 54 J/cm^2, 100 mW, diameter of 2 mm, 9 min	Salomao et al., 2015
CNV	Ophthalmology	Chinchilla Bastard rabbits	Verteporfin®, DLI 10 min, 689 nm, 1.25–10 J/cm^2, 600 mW/cm^2 for 2–33 s or 100 mW/cm^2 for 6–200 s	Framme et al., 2006a
CNV	Ophthalmology	Albino rabbits	ICG, DLI 30s or 5 min, 808 nm, 3.8 J/cm^2, 39–53 mW/cm^2, 100 s	Sawa et al., 2004
CNV	Ophthalmology	Albino rabbits	ATX-S10(Na) (13,17-bis[1-carboxypropionyl] carbamoylethyl-8-etheny-2-hydroxy-3-hydroxyiminoethylidene- 2,7,12,18-tetranethyl 6 porphyrin sodium), DLI immediately-2 weeks, 670 nm, 7.6–210.1 J/cm^2, 39–53 mW/cm^2, 1–27.5 min	Gohto et al., 2001
CNV	Ophthalmology	Pigmented Fauve de Bourgogne rabbits	WST-11 (Padeliporfin, Stakel®), DLI 1–60 min, 753 nm, 25 J/cm^2 or 50 J/cm^2, 300 mW/cm^2 or 600 mW/cm^2, 83 s	Berdugo et al., 2008
Intraocular tumors	Ophthalmology; Oncology	Pigmented rabbits (Strain: Not mentioned)	HpD, DLI 24 h or 48 h, 630 nm, 36–180 J/cm^2, 150 mW/cm^2	Gomer et al., 1985
Fungal keratitis	Infection	New Zealand White rabbits	AIEgens (IQ-TPE-2O、IQ-Cm and IQ-TPA), DLI 10 min, 689 nm, 36 J/cm^2, 20 mW/cm^2, 30 min (repeated five times)	Zhou et al., 2021
Nontuberculous mycobacteria keratitis	Infection	New Zealand White rabbits	MB, DLI 5–30 min, 650 nm, 97.5 J/cm^2, 125 mW/cm, 13 min	Shih & Huang, 2011
Papilloma	Infection; Oncology	Dutch-belted and New Zealand rabbits	ALA, DLI 3–6h, 630 nm, 40–60 J/cm^2, 100 mW/cm^2	Lofgren et al., 1995
Onychomycosis	Infection	New Zealand Albino rabbits	MB-Au NPs, 650 nm, 80 or 100 J/cm^2, 70 mW/cm^2, 19.04 min or 23.8 min (repeated four times)	Tawfik et al., 2016
Osteomyelitis	Infection	New Zealand Albino rabbits	LD4 (20-tetra{4-[(S)-2, 6-diamino-hexamide] phenyl} porphyrin), DLI 30 min, 650 nm, 95 J/cm^2, 158 mW/cm^2, 15 min	Yin et al., 2022
Bacterial Keratitis	Infection	New Zealand White rabbits	Toluidine Blue, DLI 10 min five times, 635 nm, 15 J or 30 J, 87.8 mW/cm^2, 30 min	Su et al., 2020
Balloon injury	Cardiovascular	New Zealand White rabbits	NPe6 (talaporfin sodium), DLI 1 h, 664 nm, 30 or 10 J/cm^2, 20–40 mW/cm^2	Nagae et al., 2001

Continued

Disease	Specialty	Animal	PDT regimen	References
Balloon injury	Cardiovascular	New Zealand White rabbits	ZnPc, DLI immediately, 600–700 nm, 300 J/cm^2, 180 mW/cm^2	Visona et al., 2000
Balloon injury	Cardiovascular	Watanabe Heritable Hyperlipidemic (WHHL) and New Zealand White rabbits	ALA, DLI 2h or ALA-ethyl, DLI 9h, 635 nm, 50–150 J/cm^2, 31 mW/cm^2	Kwon et al., 2008
Balloon injury	Cardiovascular	Japanese White rabbits	HpD, DLI 24 h, 635 nm, 27 mJ/cm^2, 10 min and with a repetition rate of 2 Hz (1 200 flashes).	Usui et al., 1999
Balloon injury	Cardiovascular	New Zealand White rabbits	5-ALA, DLI 2h, 635 nm, 50 J/cm^2, 210 mW/cm^2, 8–15 min	Peng et al., 2011
Esophageal varices	Gastroenterology	New Zealand White rabbits	Photofrin® (porfimer sodium), 635 nm, 90–270 J/cm^2, 300 mW/cm^2, 5–15 min	Nagamine et al., 2002
Varices	Gastroenterology	Norfolk rabbits	Photogem® (a hematoporphyrin derivative), DLI immediately, 635 nm, 48 J/cm^2, 100 mW/cm^2, 8 min	Buzzá et al., 2019
HS	Dermatology	New Zealand White rabbits	5-ALA-gels, DLI 6h, 635 nm; 5 J/cm^2, 40 mW/cm^2, 10 min (repeated four times)	Zhang et al., 2019
HS	Dermatology	Japanese White rabbits	MOF armored microneedles patch, DLI 12 h, Xe lamp (>420 nm), 30–50 mW/cm^2, 5 min	Chen et al., 2023
HS	Dermatology	New Zealand White rabbits	5-ALA, DLI 3 h, 635 nm, 114.6 J/cm^2, 20 min	Wang et al., 2014
HS	Dermatology	New Zealand White rabbits	IR-808, DLI 3 h, 808 nm, 2 W/cm^2, 120 s	Yu et al., 2022
Head and Neck Cancer	Oncology	New Zealand White rabbit	Porphyrin lipoprotein-mimicking NPs, DLI 24h, 671 nm, 125 J/cm^2, 200 mW (1st treatment) and 120 J/cm^2, 100 mW (2nd treatment)	Muhanna et al., 2016
Rectal tumors	Oncology	Japanese White rabbits	HMME (hematoporphyrin monomethyl ether), DLI 24 h, 630 nm, 60 J/cm^2, 100 mW/cm^2, 10 min; or 240 J/cm^2, 200 mW/cm^2, 20 min; or 360 J/cm^2, 300 mW/cm^2, 20 min	Gao et al., 2016
Brain tumor	Oncology	New Zealand White rabbit for VX-2 brain tumor model	ALA, DLI 3 h or 6 h, 635 nm, 240 J/cm^2, 500 mW	Xiao et al., 2009
Brain tumor	Oncology	New Zealand White rabbits	5-ALA, DLI 5–5.5 h, 635 nm, 15 J or 30 J, 6 mW/cm^2, 42 or 84 min (repeated every day for 2 weeks)	Bogaards et al., 2005
Breast cancer	Oncology	Japanese Big Ear rabbit	MB, DLI 4 h, 650 nm, 202 mW/cm^2, 5 min	Sun et al., 2019
Pigmented choroidal melanoma	Oncology	Immunosuppressed New Zealand Albino rabbits	CASPs, DLI 24 h, 675 nm, 20–70 J/cm^2, 150 or 165 mW/cm, max 7 min	Gonzalez et al., 1995
Pigmented choroidal melanoma	Oncology	New Zealand Albino rabbits	Verteporfin®, DLI 30 min, 692 nm, 60–120 J/cm^2, 300 or 600 or 1 000 mW/cm^2	Kim et al., 1996
Retinoblastoma	Oncology	Pigmented rabbits (Strain: Not mentioned)	Verteporfin®, DLI 16–109 min, 690 nm, 45–190 mW/cm^2, 1–3 min (repeated 2–6 times)	Kim et al., 2017
Thyroid cancer	Oncology	Beagle dogs	Porphyrin-HDL NPs, DLI 24 h, 671 nm, 100 J/cm, 100 mW/cm	Muhanna et al., 2020

CSC: Central serous chorioretinopathy; DLI: Drug light interval; RB: Rose Bengal; CNV: Choroidal neovascularization; ICG: Indocyanine green; MV6401: Indium chloride methyl pyropheophorbide; MB: Methylene blue; ALA: Aminolevulinic acid; MB-Au NPs: Gold nanoparticles that contained methylene blue; Npe6 (Talaporfin®): Mono-L-aspartyl chlorin e6; ZnPc: Zinc phthalocyanine; HpD: Hematoporphyrin Derivative; MOFs: Metal–organic frameworks; HS: Hyperplastic scarring; NPs: Nanoparticles; CASP: Chloroaluminum-sulfonated phthalocyanine; HDL: High-density lipoprotein.

of neovascular AMD (Mayo et al., 2003).

Glaucoma is a progressive optic neuropathy characterized by visual field defects, vision loss, and impaired visual function due to optic nerve damage, particularly prevalent in aging populations. Inspired by the antifibrotic properties of Verteporfin®-mediated PDT observed in AMD treatment, researchers have investigated the potential of PDT to modulate postoperative scarring in glaucoma. In a recent preclinical study, Verteporfin®-PDT was evaluated as a novel antifibrotic intervention following glaucoma filtration surgery in New Zealand White rabbits. The surgical approach involved the creation of a follicle via tube-channel sclerotomy. Thirty days postoperatively, assessment of follicle survival, intraocular pressure, and follicle histology and morphology revealed that PDT enhanced follicle survival and exhibited a favorable safety profile. However, its antifibrotic efficacy was inferior to that of mitomycin C (MMC), a standard adjunctive agent used to inhibit postoperative fibrosis (Sun et al., 2024). Earlier efforts explored the use of PDT to induce ciliary body edema, infarction, and necrosis in refractory glaucoma (Hill et al., 1995). Additionally, PDT has been investigated in the context of posterior capsular opacification (PCO), a common postoperative complication of cataract surgery attributable to proliferation and migration of lens epithelial cells (LECs). Rose Bengal-based PDT effectively alleviated PCO in rabbit models by selectively ablating remnant LECs following intraocular lens implantation (Koh et al., 2002). Interestingly, the vaso-occlusive effects of PDT have also been utilized to establish a rabbit branch retinal vein occlusion (BRVO) model (Li et al., 2024). However, many of these studies relied on young rabbits (10–12 weeks old, 1.8–2.2 kg), which do not accurately reflect the age-dependent pathophysiology of cataracts and glaucoma in humans. Age-related alterations in ocular structure, metabolism, and pharmacodynamics may significantly influence disease progression and therapeutic response. While rabbit models offer valuable insights into specific aspects of human eye diseases, their predictive utility for clinical outcomes remains somewhat limited due to

species-specific differences in wound healing, immune response, and drug metabolism compared to humans.

Rabbit models for cardiovascular research of PDT

Atherosclerosis, characterized by the accumulation of atheromatous plaques within blood vessel walls, leads to the progressive luminal narrowing and can ultimately result in life-threatening cardiovascular events. Owing to their distinct lipoprotein metabolism, rabbits offer key physiological advantages over rodents in modeling human-like atherogenesis and are widely used in the preclinical evaluation of PDT in cardiovascular diseases (Fan et al., 2015). While healthy rabbits typically exhibit low plasma LDL levels, administration of a high-cholesterol diet (e.g., 1%–2% cholesterol-enriched chow) rapidly elevates LDL concentrations to account for over 70% of total plasma cholesterol, closely replicating hyperlipidemic conditions observed in humans (Fan et al., 2015). Numerous studies have demonstrated that PS, such as HpD, BPD-MA, phthalocyanine, and 5-ALA, preferentially accumulate within atherosclerotic plaques in rabbits at significantly higher concentrations than in adjacent healthy vasculature (Allison et al., 1997; Eldar et al., 1990; Kwon et al., 2008; Spears et al., 1983). In one model, New Zealand White rabbits were fed a 2% cholesterol diet for five months to induce advanced atherosclerotic lesions, which were subsequently treated with PDT (Spears et al., 1983). The intervention effectively reduced plaque burden with negligible damage to surrounding vascular tissue. Inhibition of vascular smooth muscle cell (SMC) migration and proliferation can effectively reduce the occurrence of atheromatous plaques and restenosis after coronary interventions (e.g., balloon angioplasty, directional atherosclerotic resection, excimer laser angioplasty, and iliac artery stenting) (Ross, 1986). PDT has shown promise in modulating these pathological processes. Usui et al. (1999) established a rabbit model of vascular injury by introducing a 4.0 French Fogarty balloon catheter into the right common iliac artery via the femoral artery. The balloon was inflated and retracted three times to create reproducible intimal injury. Subsequent PDT application induced apoptosis in SMCs and attenuated intimal hyperplasia (IH), highlighting its potential to mitigate restenosis (Usui et al., 1999). Further supporting evidence comes from studies using zinc phthalocyanine (ZnPc) as a PS, which reached peak vascular accumulation 30 min after local administration. In an experimental model of arterial injury, ZnPc-mediated PDT reduced IH and the intima/media ratio (IMR), reinforcing its therapeutic relevance in preventing post-intervention restenosis (Visona et al., 2000). Rabbits have a suitable body size that allows for the implantation of oversized stents in the iliac arteries, providing a reliable model to simulate in-stent restenosis. In another investigation of plaque progression, an inflammatory atherosclerosis model was established in the common carotid arteries by combining balloon-induced injury with a high-cholesterol diet (Peng et al., 2011). In addition, the Watanabe Hereditary Hyperlipidemia (WHHL) rabbit, which spontaneously develops moderate to severe atherosclerosis within 6 months of birth, has also been used to investigate PS plasma distribution, arterial accumulation, and therapeutic efficacy of PDT in atherosclerotic conditions (Allison et al., 1997).

Rabbit models for gastroenterological research of PDT

Rabbits have also been instrumental in exploring the therapeutic feasibility of PDT for gastrointestinal disorders, particularly in the context of esophageal varices. These models provide valuable data for investigating underlying mechanisms, optimizing treatment regimens, and assessing clinical applications (Li et al., 2009). The marginal ear vein of rabbits has frequently been selected as an analog for human micro-varicose veins due to its comparable vessel diameter and accessibility (Buzzá et al., 2019). In one study, Photofrin®-based PDT treatment was applied using different PS doses and light exposure durations. to evaluate changes in hemodynamics and tissue morphology. Although endoscopic PDT effectively ablated targeted tissue, it also induced collateral damage to surrounding structures, raising concerns about potential variceal rupture and hemorrhage (Nagamine et al., 2002). In contrast, Photogem®-mediated PDT significantly reduced vessel length and surface temperature in the rabbit ear without causing severe histological injury, demonstrating improved safety and vascular selectivity (Buzzá et al., 2019). In addition, local irradiation with a copper vapor laser after intravenous injection of hematoporphyrin monomethyl ether led to venous endothelial disruption, thrombosis, and eventual vascular occlusion. In a limited clinical context, this approach resulted in regression of esophageal varices and reduction in endoscopic indicators of bleeding risk, including disappearance of the ‘red sign’ and reduced ulcer formation (Li et al., 2003). These findings suggest that PDT may offer a minimally invasive strategy for managing small, tortuous varices, such as esophageal varicose veins. Beyond gastrointestinal applications, rabbit models have also been employed in airway research due to the anatomical and structural similarities between rabbit and human respiratory tracts. A reliable model of airway stenosis can be established by surgically exposing the laryngotracheal tube via a midline neck incision, performing a lateral tracheal cut encompassing two-thirds of the circumference, and inserting a nylon brush to scrape the mucosa (Nakagishi et al., 2008). This model has proven effective for studying the pathophysiological mechanisms underlying airway stenosis and for evaluating the therapeutic effects of PDT in tracheal and laryngeal obstruction (Nakagishi et al., 2005).

Rabbit models for infectious disease research of PDT

The growing threat of antibiotic resistance has intensified the search for alternative antimicrobial strategies. PDT has emerged as a promising alternative approach for treating localized infections, particularly in the context of multidrug-resistant pathogens, due to its reliance on light activation. This mechanism confers several advantages, including strong targeting, broad antimicrobial spectrum, minimal risk of resistance development, and limited systemic toxicity (Mahmoudi et al., 2018), with efficacy against a wide range of pathogens, including gram-positive and gram-negative bacteria, fungi, parasites, and viruses. However, its clinical application remains largely confined to localized infections, such as those affecting the eye, skin, mucous membranes, periodontium, and dental root canals, due to limited tissue penetration, local phototoxicity, and dependence on external light exposure (Silva et al., 2015).

Rabbit models have been widely employed in preclinical PDT research to evaluate the antimicrobial effects of PS, characterize host tissue responses, and optimize therapeutic protocols for infectious diseases. Zhou et al. (2021) developed a rabbit model of bacterial keratitis by injecting a suspension

of *Staphylococcus aureus* into the corneal stroma. A mitochondria-specific aggregation-induced emission luminogen (AIEgens) was used as the PS, with PDT demonstrating significant antibacterial effects with minimal collateral damage, supporting its therapeutic potential in Gram-positive ocular infections (Zhou et al., 2021). In another study, toluidine blue-mediated PDT, combined with levofloxacin eye drops, was applied to corneal lesions in rabbits. Irradiation at 630 nm (87.8 mW/cm^2 for 30 min) effectively relieved conjunctival congestion and corneal ulceration induced by bacterial keratitis, indicating a synergistic benefit of PDT with conventional antibiotics (Su et al., 2020). PDT has also shown utility against gram-negative bacteria, such as *Mycobacterium avium*, in rabbit models of infectious keratitis (Shih & Huang, 2011). Beyond ocular infections, PDT has shown efficacy in treating deeper tissue infections such as osteomyelitis. In a rabbit tibial osteomyelitis model induced by drug-resistant *Staphylococcus aureus*, repeated PDT using the PS LD4 effectively inhibited bacterial proliferation, reduced bone destruction, and facilitated structural repair (Yin et al., 2022). These findings highlight the potential of PDT for managing refractory infections involving bone and soft tissue. PDT also shows significant potential in antiviral therapy. For example, ALA-PDT effectively reduced human papillomavirus (HPV) infections in rabbits, reducing viral load and lesion recurrence without causing significant side effects on the skin (Lofgren et al., 1995).

Rabbit models for dermatological research of PDT

Rabbits are extensively utilized in dermatological PDT research due to their anatomical and physiological similarities to human skin, including comparable epidermal and dermal structure, skin thickness, cellular composition, sensitivity to stimulation, ease of experimental manipulation, and reproducibility (Mapara et al., 2012). The rabbit ear provides a well-established platform for studying transdermal PS penetration and accumulation, allowing direct visual and histological assessment following topical application. Traditional treatments for cutaneous conditions such as hypertrophic scars (HS) —such as surgical excision, laser ablation, and corticosteroid injections —are often associated with limited efficacy, high recurrence rates, and pain (Monstrey et al., 2014). PDT, through the generation of ROS, offers a promising, non-invasive alternative by promoting apoptosis of hypertrophic scar fibroblasts (HSFs) and degrading excess collagen and extracellular matrix (ECM). For instance, combining PDT with tissue inhibitor of metalloproteinases (TIMP)-1 has been shown to accelerate HSF senescence and enhance therapeutic outcomes in rabbit models (Wang et al., 2014). Moreover, the integration of nanomedicine into PDT has significantly improved transdermal PS transport by overcoming the ECM barrier of HS, enabling effective dermal penetration, induction of HSF apoptosis, and marked improvements in scar appearance and collagen fiber remodeling (Wang et al., 2014). Nanoethosome, composed of phospholipids, ethanol and water, is an innovative nanoscale lipid carrier primarily designed to enhance the transdermal delivery of drugs and active ingredients. Nanoethosome exhibits greater flexibility and permeability than traditional liposomes. Zhang et al. (2019) prepared 5-ALA-loaded nanoethosome (ALA-ES) gels which could deliver 5-ALA to HSF in rabbit HS tissues by transdermal administration and convert it into protoporphyrin IX that induces PDT. Moreover, it was found that irradiation could lead to the accumulated protoporphyrin IX to ameliorate HS by inducing cell death in HSFs and remodeling collagen fibers. The HS model in this study was established using the Morris method, involving the creation of 10 mm circular wounds on the ventral surface of the rabbit ear to simulate human proliferative scarring (Morris et al., 1997). Alternative PS systems have also been evaluated for topical PDT applications. For example, Rose Bengal-hydrogel formulations were applied to the shaved dorsal skin of rabbits, with or without light irradiation. Results revealed that Rose Bengal accumulated in the epidermis and hair shafts, with minimal penetration into deeper tissues and no significant evidence of phototoxicity or thermal damage, indicating a favorable safety profile for dermatological use (Wachter et al., 2003). To overcome limitations in transdermal PS delivery and address autophagy-mediated resistance to PDT, researchers developed a microneedle patch incorporating a metal-organic framework (MOF) structure encapsulated with an autophagy inhibitor, which showed enhanced PS penetration and improved scar repair in a rabbit ear model (Chen et al., 2023). Similarly, Yu et al. (2022) engineered multilayered nanoethosomes loaded with the PS IR-808 (IR-808-ES) for combined PDT and photothermal therapy (PTT). This dual-modality approach enhanced transdermal delivery and significantly improved therapeutic outcomes in HS treatment.

The rabbit VX2 tumor model has been widely employed in PDT research to evaluate the antitumor efficacy, tissue selectivity, and systemic safety of novel PS. VX2 tumors are morphologically and biologically similar to human malignancies, including overexpression of LDLR (Pascale et al., 2022). Tumors can be established by injecting VX2 tumor cell suspensions into rabbit muscle or bone, resulting in the formation of palpable tumors within approximately 2 weeks (Cao et al., 2018; Handal et al., 2013). Alternatively, VX2 *in situ* tumor models can be constructed by surgically implanting VX2 tumor tissue into specific organs such as the liver or kidneys, enabling assessment of site-specific PDT responses (Eifler et al., 2009; Kim et al., 2017; Muhanna et al., 2020; Shafirstein et al., 2018). Experimental protocols typically involve serial blood sampling before and after PS administration and PDT treatment, biochemical and hematological analyses, postoperative pathological analysis of tumors and normal organs, and survival time of tumor-bearing rabbits to evaluate the toxicity and antitumor efficacy of PDT. Rabbit models have also been used to study PDT in the treatment of skin cancers such as basal and squamous cell carcinoma (Muhanna et al., 2020).

While rabbit models offer distinct advantages, such as anatomical adaptability, surgical feasibility, and compatibility with a wide range of experimental endpoints, they also present notable limitations. Species-specific metabolic differences, particularly in cytochrome P450 enzyme profiles, can alter the pharmacokinetics of certain PS (e.g., porphyrins), potentially leading to biased predictions of toxicity or efficacy (Bogaards et al., 2000; Kumar et al., 2009). Furthermore, the scarcity of spontaneous tumors in rabbits necessitates reliance on transplantable VX2 models, which lack the complexity of human tumor microenvironments and limit the potential for clinical translation of PDT (Pascale et al., 2022). Optical interference from fur or melanin may also compromise light penetration, requiring depilation or the selection of albino

strains for improved PDT delivery. To enhance the translational value of rabbit models in PDT, research should prioritize the construction of a more accurate, dynamic, and ethically compliant research system through genetic engineering, multimodal imaging, and computational biology. Adoption of the 3R principles, “Replacement, Reduction, and Refinement”, should be actively promoted in the field of PDT via organoid-rabbit and computational modeling.

DOG MODELS IN PDT RESEARCH

Dogs represent a valuable non-rodent model in the preclinical evaluation of PDT, especially in pharmacological and toxicological assessments of PS (Durrani et al., 2023; Payne et al., 1996). As one of the most commonly used non-rodent species in regulatory studies, dogs—especially Beagles—are internationally recognized for their utility in bridging translational gaps between rodent data and human clinical trials (Foster et al., 2022). Regulatory agencies, including the European Medicines Agency (EMA) and US Food and Drug Administration (FDA), generally require toxicity testing in both rodents and non-rodent mammals prior to human administration to provide more reliable and predictive data and ensure comprehensive safety evaluation (Haitina et al., 2009). Previous research has investigated the toxicokinetic and toxicological effects of a chlorophyll-derived PS, [(methyl-3-(1’-meta-iodo-benzyloxy) ethyl-3-devinylpyropheophorbide-a], in rats and beagles, with the highest PS dose without observed adverse effects found to be 6.55 mg/kg and 3.45 mg/kg, respectively (Cacaccio et al., 2022). Similarly, the pharmacokinetics and toxicity of Photobac were evaluated across mice, rats, and dogs, demonstrating comparable systemic exposure and minimal toxicity in both rodents and canines (Durrani et al., 2023). As shown in Table 2, these findings emphasize the importance of large animal models in characterizing the physicochemical behavior, biodistribution, and safety of PS under clinically relevant conditions.

Rodent models, including subcutaneous and orthotopic tumor xenografts, are frequently employed to investigate PDT efficacy in superficial or small-volume tumors, such as cutaneous malignancies and head and neck squamous cell carcinoma (Silva et al., 2015). However, these models are limited in their ability to simulate the anatomical depth and tissue complexity of larger organs, such as the prostate, kidney, and stomach. In contrast, canine anatomy, particularly the skin, mouth, and lungs, closely approximates that of humans, providing a more suitable model for assessing light penetration and tissue distribution of PDT in humans. Additionally, dogs naturally develop a range of spontaneous tumors, including melanoma and squamous cell carcinoma, which exhibit pathological features such as angiogenesis, stromal architecture, and immune microenvironment comparable to those of human malignancies (Hytönen & Lohi, 2016). These spontaneously arising tumors enable clinically relevant investigations into PDT efficacy, resistance mechanisms, and combinatory regimens. Notably, previous studies have evaluated the comparative therapeutic efficacy and safety of conventional surgery (rectal resection and low rectal end-to-end anastomosis) and PDT in canine models of rectal cancer. Findings indicated that PDT may serve as a viable adjunct to surgery and radiotherapy. In this protocol, motexafin lutetium was administered intravenously at a dose of 2 mg/kg, followed by laser irradiation at 730 nm, delivering a light fluence of 0.5–10 J/cm^2 three hours post-injection (Ross et al., 2006). These findings align with observations from a Phase I clinical trial investigating motexafin lutetium in prostate cancer, where patients received doses ranging from 0.5 to 2.0 mg/kg and light fluences of 25–150 J/cm^2 at intervals of 3–24 hours post-administration, showing excellent tolerance with no serious dose-limiting toxicities (Du et al., 2006).

Dogs offer unique translational advantages for PDT research due to their anatomical size, physiological similarity to humans, and amenability to clinical imaging and surgical techniques. Their body size permits the use of clinical-grade diagnostic and therapeutic equipment, including endoscopy, magnetic resonance imaging (MRI), and positron emission tomography-computed tomography (PET-CT), enabling real-time evaluation of PS distribution, PDT efficacy, and treatment-associated tissue damage (Chang et al., 1999; Chevalier et al., 2011, 2013; Lucroy et al., 2003; Swartling et al., 2016; Xiao et al., 2007). In one illustrative study, laser irradiation delivered via a transurethrally or transperineally inserted fiber significantly inhibited spontaneous prostate tumors in dogs without compromising the structural integrity of the prostate body, demonstrating both efficacy and safety in a large-animal model of human prostate cancer (Chang et al., 1996). With an average lifespan of 10–15 years, dogs are also well-suited for studying long-term safety outcomes of PDT, such as skin phototoxicity, and for investigating mechanisms of tumor recurrence and treatment resistance (Osaki et al., 2012). Their close anatomical and histopathological resemblance to humans —particularly in periodontal tissue architecture, disease progression, and underlying etiological factors —makes dogs a highly relevant model for studying periodontal disease (Madi & Alagl, 2018). For example, a previous study established a canine model of periodontal infection by introducing *Porphyromonas gingivalis* and *Clostridium nucleatum* into the subgingival and supragingival regions, including the vestibule and posterior tongue, to evaluate the efficacy of Ce-6-mediated PDT in reducing bacterial load and alleviating periodontal redness and bleeding (Sigusch et al., 2005). Beyond infection control, PDT has been applied to support guided bone regeneration, with its effects evaluated in a canine model of chronic implant-associated osteochondritis dissecans (Ramos et al., 2017). Similarly, in a canine model of chronic peri-implantitis, De Oliveira et al. (2011) reported that PDT reduced the expression of several inflammatory cytokines, such as tumor necrosis factor α (TNF-α), NF-kB receptor activator ligand (RANKL), osteoprotegerin (OPG), matrix metalloproteinase (MMP-1), interleukin-6 (IL-6), and IL-10, as well as bacterial load, supporting its anti-inflammatory and antimicrobial properties in peri-implant disease. Although other large-animal models, including NHPs, minipigs, and sheep, have also been used to explore the antimicrobial capacity of PDT in peri-implantitis, dogs remain the most frequently used species for investigating PDT-based interventions in oral and periodontal pathologies (Hanisch & Kettenmann, 2007; Hickey et al., 1991; Singh, 1993). In veterinary clinical practice, PDT has been investigated for managing a wide range of localized refractory bacterial infections in dogs, including chronic otitis, multiple types of cancers and sarcomas, chronic gingivostomatitis, and dermatophytosis (Abreu Villela et al., 2017; Cabral et al., 2021; De Nardi et al., 2023; Guidi et al., 2021; Jacobs & Rosen, 2000; Osaki et al., 2019, 2023; Sellera et al., 2019). These studies expand the use of PDT in veterinary medicine

Table 2 Dogs used in PDT research

Disease	Specialty	Animal	PDT regimen	Results	References
Chronic otitis	Infection	Lhasa apso dog	MB, DLI 5 min, 660 nm, 140 J/cm^2, 3.5 W/cm^2	• Complete clinical resolution by day 7 post-intervention, with absence of foreign bodies, exudate, or tympanic membrane pathology on otoscopic evaluation. • Potent bactericidal activity against *Pseudomonas aeruginosa* ATCC 27853 and *P. aeruginosa* ICBDVIM-2 strain *in vitro*.	Sellera et al., 2019
Chronic gingivostomatitis	Infection	Healthy pigs	MB, 660 nm, 7.2 J/point, 3 min/point, 180 J/cm^2, spot size of 0.04 cm^2	• Decrease of petechiae in buccal mucosa on day 15 post-intervention, with slight recurrence by day 30 post-intervention. No significant histopathogical changes. • No recurrence of lesions after second irradiation.	Abreu Villela et al., 2017
Dermatophytosis	Infection	Pekingese dog	MB, DLI 10 min, 650 nm, 30 J/cm^2 (6 J and 150 s per point, total of 4 points, spot size 0.2 cm^2), 40 mW	• Decrease of petechiae in buccal mucosa on day 15 post-intervention, slight recurrence by day 30 post-intervention. • No significant histopathogical changes.	Cabral et al., 2021
Peri-implantitis	Infection	Silk ligatures placement-induced peri-implantitis in Beagle dogs	Phenothiazine chloride, DLI 5 min, 660 nm, 44 J/cm^2, 212 mW/cm^2, 30 s	• Lesions were significantly reduced by 4-fold with small circular patches at 7 days post-treatment. • Approximately 90% reduction of upper lesion with small wound and no wound in lower lesion at 14 days post-treatment. • No erythema or inflammatory signs at 21 days post-treatment. • Hair regrowth around lesions 1 month after healing, and complete coverage after 2 to 6 months.	Ramos et al., 2017
Chronic rhinosinusitis	Infection	Cross-breed dog	Verteporfin®, DLI 15 min, 690 nm, 200 J/cm, 250 mW/cm	• Decreased soft tissue opacity and resolved clinical signs at 11 days post-treatment. • Mucopurulent nasal discharge at 18 days post-treatment. • Recurring facial swelling, reverse sneezing and CT showed bilateral soft tissue opacity at 107 days post-treatment. • Recurrence at 381 days post-treatment. • Euthanized at 569 days post-treatment.	Osaki et al., 2012
Periodontitis	Infection	Beagle dogs	Ce6 or BLC1010, DLI 5 min, 662 nm, 0.5W–2.5W, 12.7 J/cm^2 per site, 3.3 s per site, spot size of 0.13 cm^2	Significantly reduced porphyromonas gingivalis-infected sites, while less significant reduction of fusobacterium nucleatum-infected sites at 2 weeks post-treatment.. • Significantly reduced redness and bleeding on probing (BOP).	Sigusch et al., 2005
Spontaneously occurring tumors (melanoma, hemangiopericytoma, squamous cell carcinoma)	Oncology	Pet Dogs	G-Ce6, DLI 5 min, 677 nm, 50–150 J/cm^2, 200–300 mW/cm^2 by flat-cut fibers or 90–150 J/cm, 160–200 mW/cm by quartz fibers	• Repeated VTP sessions achieved complete remission (CR) in three dogs, stable disease (SD) in one, and progressive disease (PD) in one. • Short half-life for G-Ce6, suggesting reduced skin photosensitization. • Complications during treatment, including edema of surrounding normal tissue and fistulae.	Osaki et al., 2023
Solid tumors and sarcoma	Oncology	Pet dogs and cats	5-ALA, DLI 4 h, 630 nm, 20–300 J/cm^2, 50 mW/cm^2 or 150 mW/cm^2 or 200 mW/cm^2 (repeated PDT for 2–16 times)	• Red fluorescence of 5-ALA observed in 88.8% of malignant tumors. • Repeated PDT significantly reduced tumor size and achieved long-term tumor control when combined with chemotherapy. One dog with adenocarcinoma of left paranasal sinus achieved complete remission after 15 PDT sessions and survived for 718 days. • Cytotoxicity of 5-ALA-PDT in carcinomas correlated with intracellular PpIX concentration *in vitro*.	Osaki et al., 2019
Esophageal squamous cell carcinoma	Oncology	Labrador dog	Porfimer sodium, DLI 48h, 630 nm, 200 J/cm^2	• Three times repeated PDT under endoscopic guidance over 2 months resulted in reduction in tumor size and return of oral alimentation. • Euthanized 9 months after onset of therapy due to cancer metastasis.	Jacobs & Rosen, 2000

DLI: Drug light interval; Ce6: Chlorin e6; G-Ce6: Glucose-conjugated chlorin e6; ALA: Aminolevulinic acid.

and contribute to preclinical translational research for the diagnosis and treatment of human diseases.

Dog models offer distinct anatomical and translational advantages in PDT research, especially in spontaneous tumor and clinical-grade device validation. However, their role as companion animals presents ethical challenges that necessitate rigorous oversight and thorough justification of alternatives (MacEwen, 1990). Additional barriers include high maintenance costs, limited availability of spontaneous cancers, and interspecies metabolic differences—for instance, the absence of hepatic aldehyde oxidase—which may affect drug metabolism and limit extrapolation to human oncological settings (Martinez et al., 2021). There is a need to improve the accuracy and ethical compliance of these models through genetic engineering, multimodal monitoring, and natural cohort studies, as well as to promote the development of “virtual” dog organs and tissues (e.g., mini-organs or organoids) to assess toxicity in place of real animals, thereby maximizing the clinical translational potential of PDT technology.

PIG MODELS IN PDT RESEARCH

Pigs have emerged as a pivotal large-animal model in PDT research, particularly for evaluating the toxicity and pharmacokinetics of PS (Figure 3, Table 3). Their organ size, vascular structure, immune function, and metabolic characteristics provide an experimentally accessible platform for FDA-approved Phase I human clinical trials (Durrani et al., 2023; Gutierrez et al., 2015).

The cardiovascular system of pigs, including coronary anatomy and blood flow dynamics, is very similar to that of humans, highlighting their clinical relevance in studies targeting vascular responses to PDT. Their lipoprotein metabolism, marked by LDL and HDL profiles similar to those of humans, adds further value in modeling lipid-related pathologies, such as atherosclerosis, obesity, and diabetes (Gallardo et al., 2008; Kaabia et al., 2018). For example, histological and immunohistochemical analyses of arterial tissue following PDT have indicated that treatment can mitigate intimal hyperplasia at vascular anastomosis sites (Heckenkamp et al., 2007). Comparative studies have also revealed species-specific differences in the pharmacodynamic behavior of PS. Notably, Tremblay et al. (2003) investigated endobronchial phototoxicity and vascular responses to WST-09 (Tookad®)-mediated PDT in Large White-Landrace male piglets. At a dose of 2 mg/kg, the duration of skin photosensitivity and vascular reactivity was approximately 3 hours in rats but less than 1 hour in pigs, indicating more rapid systemic clearance in the porcine model. This pharmacokinetic profile suggests a reduced risk of prolonged phototoxicity of WST-09 compared to first-generation agents such as Photofrin®. Building on the structural and immunological resemblance of minipig skin to that of humans, Wei et al. (2024) applied Janus liposome-assisted PDT in a diabetic wound infection model, demonstrating effective antimicrobial activity and accelerated tissue repair. Additionally, chlorin e6 (Ce6)-embedded intragastric satiety-inducing devices (ISDs) have been evaluated in both juvenile and miniature pigs, confirming their safety and therapeutic potential for noninvasive obesity treatment (Kim et al., 2023; Park et al., 2024).

An additional advantage of porcine models in PDT research lies in their organ size and anatomical proportions, which permit direct use of clinical-grade light delivery systems and fiber-optic devices without requiring substantial modification (Bae et al., 2014; Siewerdsen et al., 2005). In contrast, PDT instrumentation for murine models often necessitates extensive adaptation to approximate clinical use. Van Staveren et al. (1997) employed *ex vivo* pig bladders to evaluate the impact of eccentric light-source positioning on intravesical light dosimetry. Similarly, intra-arterial delivery of 5-ALA for PDT has been demonstrated using a conventional

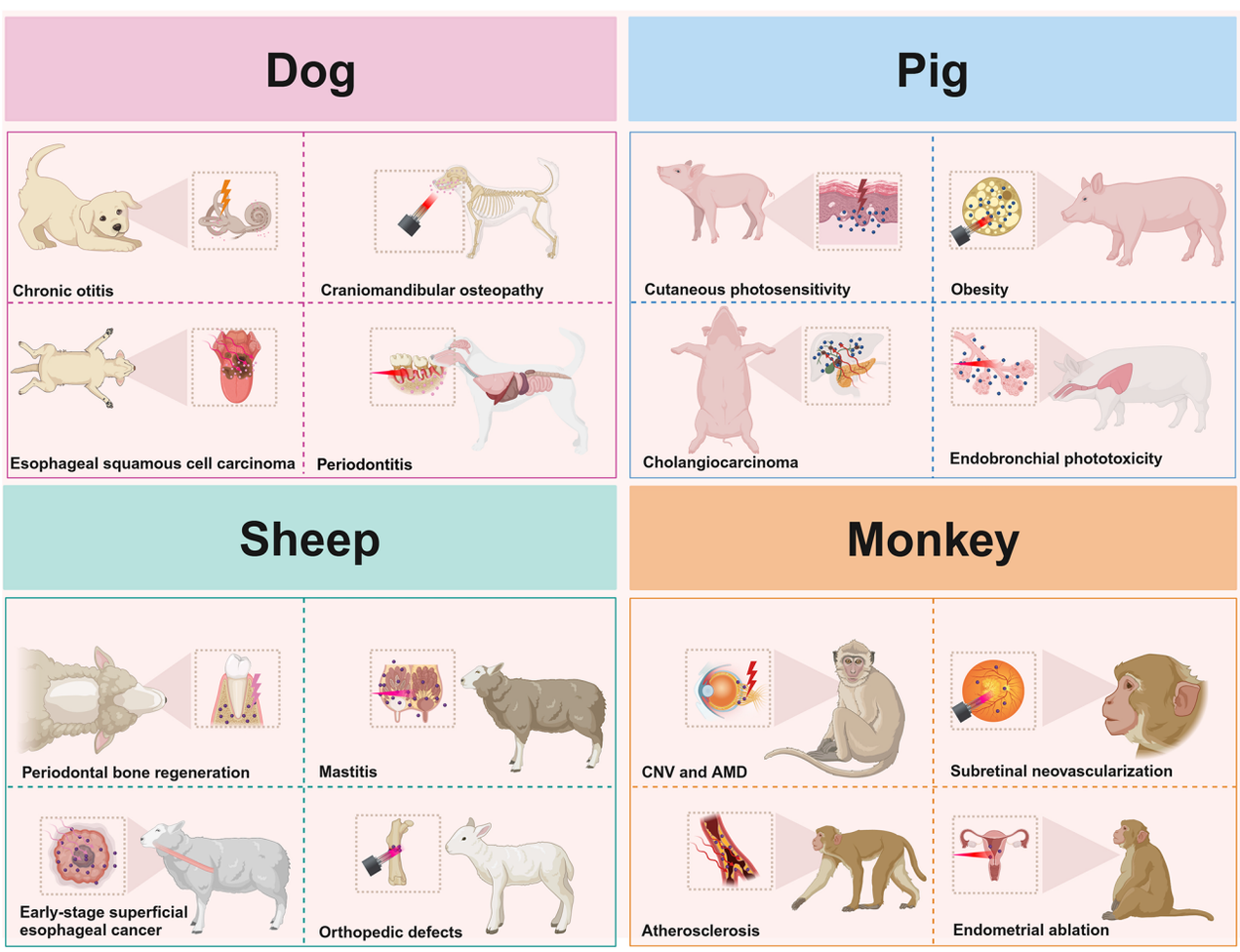

Figure 3 Utilization of large animal models (dogs, pigs, sheep, and NHPs) in PDT research, demonstrating translational potential for various diseases

Figure created with BioRender.com.

Table 3 Pigs, sheep, and monkeys used in PDT research

Aim of study	Animal model	PDT regimen	References
Restenosis post-angioplasty	White pig non-injury model	5-ALA, DLI 1.5 h/2.5 h/6–7 h, 635 nm, 50 J/cm^2	Jenkins et al., 1998
Cutaneous photosensitivity of PS	Healthy pigs	WST-09, DLI 1–3 h or longer, full solar spectrum, 128 J/cm^2	Weersink et al., 2005
Endobronchial phototoxicity of PS	Healthy Large White-Landrace male pigs	WST-09, DLI 5–15 min, 763 nm,100/200/300 J/cm², 60/320 mW/cm²	Tremblay et al., 2003
Esophageal strictures induced by PDT for Barrett's esophagus	Healthy pigs	Photofrin®, DLI 48 h, 630 nm, 400 J/cm^2	Perry et al., 2005
Intimal hyperplasia in prosthetic vascular by PDT	Porcine PTFE bypass model	MB, DLI 5 min, 660 nm, 150 J/cm^2, 100 mW/cm^2	Heckenkamp et al., 2007
PDT for Wound healing	Bama miniature pig infected diabetic wounds	Janus liposozyme, DLI 3 min, white light, 10 J/cm^2, 24 mW/cm^2, 10min	Wei et al., 2024
PDT for obesity	Mini pig	Ce6-embedded intragastric satiety-inducing device (ISD), 660 nm, 200 J/cm^2, 1 000 mW/cm^2	Park et al., 2024
PDT for obesity	Mini pigs	Ce6-embedded intragastric satiety-inducing device (ISD), DLI 24 h, 670 nm, 1 or 5 J/cm^2, 50 mW/cm^2	Kim et al., 2023
Implantable device for PDT in brain	Domestic pigs	Globus Lucidus, 630 nm (19.5 mW/cm^2), 405 nm (5.0 mW/cm^2) or 275 nm (0.9 mW/cm^2).	Bader et al., 2024
PDT for cholangiocarcinoma	Pigs (55 kg female)	Pullulan acetate-conjugated pheophorbide A-embedded self-expanding metal stent, DLI 30 min, 690 nm, 150 J/cm^2	Bae et al., 2014
PDT for periodontal bone regeneration	Sheep	Novel biomaterials contained mTHPC, 652 nm, 830 mW/cm², 40s	Rahn et al., 1999
PDT for squamous-cell carcinoma	Sheep	FOSCAN®, DIL 4 days, 514 nm, 10 to 500 J/cm^2, 100 mW/cm²; or 413 nm, 5–250 J/cm², 13 mW/cm²	Radu et al., 2005
PDT for early superficial esophageal cancer	Sheep	FOSCAN®, 514 nm, 75–120 J/cm^2, 100 mW/cm^2, 20 min; HPD and Photofrin, 630 nm, 100-180 J/cm^2, 80–150 mW/cm^2, 20 min; Esophageal irradiations were carried out at 652 nm, 8–12 J/cm^2, 150 mW/cm^2, 20 min	Radu et al., 2003
PDT for subretinal neovascularization	Cynomolgus monkeys	RB, DIL 20 min or 45 min, 510 nm, 12.7 mW/cm^2	Miller & Miller, 1993
PDT as endometrial ablation	Rhesus and cynomolgus monkeys	5-ALA, DIL 4 h, 635 nm, 300 mW/cm^2, 60 min in either continuous or fractionated fashion	Van Vugt et al., 2000
PDT for CNV	Cynomolgus monkeys	Verteporfin®, DIL 32 min or 50 min, 689 or 692 nm, 150 J/cm^2, 600 mW/cm^2	Husain et al., 1996, 1997, 1999
PDT for CNV	Cynomolgus monkeys	HpD, DIL 40 min or 1 day or 3 days, 630 nm, 40 mW/cm^2 or 100 mW/cm^2 or 200 mW/cm^2, 10 min	Ohnishi et al., 2002
PDT for CNV	Cynomolgus monkeys	Verteporfin®, DIL 2 weeks, 689 nm, 100 J/cm^2, 600 mW/cm^2, 166.6 s (repeated PDT)	Reinke et al., 1999
PDT for CNV	Cynomolgus monkeys	Verteporfin®, DIL ND, 692 nm, 50 J/cm^2, 150 mW/cm^2 for 6min or 1800 mW/cm^2, 30 s	Miller, 2008
PDT for CNV	Cynomolgus monkeys	ATX-S10(Na), DIL 1–19 min, 670 nm, 1–86.9 J/cm^2, 6.9–437.5 mW/cm^2, 30–240 s	Obana et al., 2001
PDT for CNV	Cynomolgus monkeys	ATX-S10(Na), DIL 0–150 min, 670 nm, 1–127 J/cm^2, 6–528 mW/cm^2	Obana et al., 2000
Inhibition of NOS for photoreceptor damage caused by PDT treatment for CNV	Cynomolgus monkeys	Verteporfin®, DIL 5–100 min, 689 nm, 50 J/cm^2 over 2 min 47s or 150 J/cm^2 over 4 min 9 s	She et al., 2007
PDT in combination with anti-VEGF monoclonal antibody for CNV	Cynomolgus monkeys	Verteporfin®, DIL 15 min, 689 nm, 100 J/cm^2, 600 mW/cm^2 (repeated PDT three times)	Husain et al., 2005; Kim et al., 2006

ALA: Aminolevulinic acid; PS: Photosensitizer; MB: Methylene blue; DLI: Drug light interval; Ce6: Chlorin e6; RB: Rose Bengal; HpD: Hematoporphyrin Derivative; NOS: Nitric oxide synthase; CNV: Choroidal neovascularization; ATX-S10(Na): 13,17-bis (1-carboxypropionyl) carbamoylethyl-8-etheny-2-hydroxy-3-hydroxyiminoethylidene-2,7,12,18-tetraethyl porphyrin sodium.

percutaneous transluminal angioplasty (PTA) balloon catheter with a transparent lumen in a swine model (Jenkins et al., 1998). Endoscopic administration of PDT via laser probe, consistent with protocols used in clinical settings, has also been validated in pigs (Perry et al., 2005). Given the physiological parallels in gastric hemodynamics and inflammatory responses between pigs and humans, pig models have been established to investigate the effects of m-TPHC-mediated PDT on normal gastric tissue (Mallas et al., 2004). The combined use of PDT and transparent silicone airway stents has also been successfully evaluated in a swine model (Ohtani et al., 2020). Additionally, Bader et al. (2024) explored globus lucidus-mediated PDT and photochemical therapy at sustained low fluence rates for glioblastoma, monitoring local inflammation, edema, and intracerebral hemorrhage following implantation of the irradiation device in the porcine brain. This platform provides a foundation for advancing PDT-based strategies in neuro-oncology. Despite their theoretical applicability in oncological PDT, pig models remain underutilized due to practical constraints, including longer maturation cycle (6–12 months), rapid growth, challenges in tumor model construction, and high

maintenance costs and requirements after treatment.

In summary, pig models represent a critical bridge linking basic *in vitro* findings and human clinical trials in PDT research. However, their application requires careful consideration of physiological relevance, cost-effectiveness, and translational reliability. Advancing their utility will depend on technological innovation and interdisciplinary collaboration aimed at addressing interspecies differences, refining model fidelity, and enhancing the precision of PDT translation from experimental systems to clinical application.

NHP MODELS IN PDT RESEARCH

NHPs have been utilized in PDT research due to their close anatomical and physiological resemblance to humans, particularly in ophthalmological contexts (Table 3). The most commonly used NHPs are rhesus macaques, crab-eating macaques, African green monkeys, and squirrel monkeys. (Criswell et al., 2005; Moshfeghi et al., 1999; Van Vugt et al., 2000). The structural and functional characteristics of the NHP eye, including the cornea, lens, retina, optic nerve, and overall visual system, closely resemble those of humans, making them highly suitable for studying ocular diseases and evaluating PDT interventions. Ultrastructural analyses using transmission electron microscopy have revealed the tolerance thresholds of different eye structures, such as the outer retinal segments, retinal pigment epithelium, and vascular endothelium, following HpD-mediated PDT in cynomolgus monkeys (Ohnishi et al., 2002). The high density of cone photoreceptors in the central concave region of NHPs also facilitates studies of visual and macular degeneration (Tamaki, 2007). Additionally, the dense and complex choroidal vasculature of NHPs closely mirrors human vascular structure and hemodynamics, providing a suitable platform for modeling ocular vascular diseases (Peyman et al., 2000). In an earlier study, Miller & Miller (1993) demonstrated that rosmarinic benzyl-gal-mediated PDT effectively induced subretinal neovascular occlusion in cynomolgus monkey eyes, with minimal collateral damage to the overlying retina. Subsequent studies confirmed the efficacy of Verteporfin®-PDT in cynomolgus monkeys by demonstrating targeted occlusion of abnormal microvasculature in choroidal neovascular membranes and tumors (Husain et al., 1996; Reinke et al., 1999). Repeated low-dose Verteporfin®-PDT resulted in significantly less retinal, choroidal, and optic nerve damage compared to a single high-dose treatment. Although Verteporfin®-PDT induced photoreceptor injury in a monkey CNV model, co-administration of a nitric oxide synthase (NOS) inhibitor mitigated this effect by downregulating inducible NOS expression in macrophages (Reinke et al., 1999). Additionally, Ce6-mediated PDT outcomes in rhesus monkeys varied by retinal region, with optimal vascular responses observed beneath the central fossa and diminished effects in the macular area (Peyman et al., 2000). Although anti-VEGF therapy has largely replaced PDT in the management of neovascular age-related macular degeneration, combination strategies incorporating PDT remain under investigation (Husain et al., 2005; Kim et al., 2006; Miller, 2008). Notably, Cheong et al. (2021) recently explored the potential of epinephrine combined with Verteporfin®-PDT as a therapeutic intervention for CNV in crab-eating monkeys, enabling high-resolution evaluation of outer retinal and choroidal ultrastructure, as well as changes in luminal and stromal architecture post-treatment. Beyond ophthalmic applications, 5-ALA-PDT has been evaluated as a non-invasive alternative to endometrial ablation in rhesus monkeys, with all subjects—whether postmenopausal or in the early proliferative phase —exhibiting measurable ablation depths ranging from 1.14±0.54 to 2.15±1.62 mm (Van Vugt et al., 2000). Additionally, HpD application has demonstrated selective accumulation in atherosclerotic plaques in both rabbits and rhesus monkeys, sparing adjacent normal tissue (Spears et al., 1983).

Collectively, these findings underscore the value of NHPs as an important bridge between preclinical research and clinical medicine, with considerable value in PDT research, particularly for complex ocular diseases and long-term safety evaluations. However, their use is constrained by ethical considerations, high costs, limited reproductive capacity, and strict regulatory requirements. Future efforts should integrate NHPs into a multi-level validation system alongside pigs, zebrafish, organoids, and other alternative models to promote the efficient translation of PDT studies. When employed judiciously within ethically sound frameworks, NHPs offer a robust research platform that can drive meaningful progress in the application of PDT.

SHEEP MODELS IN PDT RESEARCH

Sheep have been employed as large-animal models in PDT research since the early 2000s, primarily to evaluate the safety and tissue responses associated with novel PS (Table 3). In particular, tetra(m-hydroxyphenyl)-chlorin (mTHPC) was investigated in sheep for its therapeutic potential in early-stage esophageal tumors (Radu et al., 2003, 2005). Notably, the esophageal anatomy of sheep, specifically the structural and thickness characteristics of the mucosal and muscular layers, more closely resembles that of humans than do rodent models, which possess a thinner esophageal wall and less developed muscular layers and glands (Liu et al., 1992). However, high-dose green light following mTHPC sensitization in sheep can lead to serious complications, including fibrosis, ring necrosis, and luminal stricture (Radu et al., 2003).

In addition to oncology applications, PDT has been explored in sheep as a topical antimicrobial. A recent study evaluated the efficacy of methylene blue-mediated PDT for the treatment of mastitis by detecting changes in microbial load in post-treatment milk samples (Silva et al., 2022). Although sheep are not routinely used in PDT studies, they present several advantages, especially in studies of oral diseases and orthopedics (Nuss et al., 2006; Pearce et al., 2007). Their skeletal and dental physiology, such as bone and joint structure, body weight, and bone mineral metabolism, closely aligns with human parameters, making them an ideal model for evaluating the efficacy of PDT in periodontitis and periodontal bone regeneration. For example, Sigusch et al. (2023) implanted a novel photoactive biomaterial into non-critical bone defects (5 mm diameter) in the femur and tibia of female domestic sheep to explore the antimicrobial surface activity of PDT for periodontal bone regeneration. Due to the uniformity in bone architecture, overlying soft tissue, and mechanical loading across defect sites, the sheep monocortical model offers a consistent and well-tolerated platform for studying bone regeneration across different healing stages (Atayde et al., 2014; Kranz et al., 2023).

Despite their advantages for studies on esophageal tumors, periodontitis, and periodontal bone regeneration, research is

limited by ethical considerations, high maintenance costs, and the need for procedural standardization and improved welfare.

OTHER MODELS IN PDT RESEARCH

Cell culture and *ex vivo* models

Cell culture systems, including both primary cells and established cancer lines, are widely used to assess PS cytotoxicity, cellular uptake kinetics, and photoactivation responses such as ROS generation (Wang et al., 2015). Conventional two-dimensional (2D) monolayers cultured on planar surfaces serve as a foundational platform for preliminary PS screening and high-throughput evaluation (Mansoori et al., 2019). To better replicate the tumor microenvironment, co-culture systems have been developed to study PS accumulation dynamics and the immunogenic consequences of PDT-treated cancer cells. For example, Lara et al. (2021) simultaneously exposed cancer cells, dendritic cells, and macrophages to PS and assessed differential uptake based on fluorescence intensity, revealing preferential accumulation in specific cell types. The capacity of PDT to trigger immunogenic cell death has also been demonstrated in co-culture systems, where immune cells responses were examined following exposure to PDT-treated tumor cells (Hao et al., 2022a, 2023b; Turubanova et al., 2019). Although 2D cell culture models offer certain advantages, such as simplicity, cost-efficiency, and ease of standardizations, they fail to replicate the physiological complexity of disease microenvironments. To address these limitations, three-dimensional (3D) culture systems have been developed, wherein cells are embedded within gel-like matrices or seeded onto solid scaffolds to better simulate native tissue architecture (Aires-Fernandes et al., 2022). These models include biologically derived construct such as organoids and spheroids, as well as engineering-based platforms such as biomaterial scaffolds and microfluidic chips, which are commonly used in PDT study, especially in oncology (Mohammad-Hadi et al., 2018). Compared to 2D systems, 3D models provide better simulation of the cellular microenvironment, including oxygen gradients and barriers to drug penetration and light diffusion (Mohammad-Hadi et al., 2018). Such platforms are essential for assessing spatial PS distribution and light attenuation in multilayered tissues (Nath & Moore, 2019). Both spheroids and organoids can mimic the structure and function of organs, enabling mechanistic investigations of PDT within biologically relevant tissue contexts. However, spheroids consist of loosely organized cell aggregates and lack higher-order functionality. In contrast, organoids are derived from stem cells and comprise multiple differentiated lineages, more accurately recapitulating the structural and functional properties of native organs (Gunti et al., 2021).

Ex vivo tissue systems from animal sources allow direct assessment of PDT effects on specific tissues or organs. These models allow for the assessment of PDT-induced damage in a more realistic tissue context. Early studies employed *ex vivo* pig bronchi to characterize light distribution in endobronchial PDT with Photofrin I (Jones et al., 2009; Marijnissen et al., 1993; Murrer et al., 1999). Subsequent studies used porcine kidney, liver, and fat to investigate PS aggregation and tissue penetration and PDT-induced singlet oxygen kinetics (Arnfield et al., 1992; Kimm et al., 2016; Schlothauer et al., 2012), showing that NIR wavelengths of 789 nm achieve 1–2 times deeper penetration than 630 nm light (Arnfield et al., 1992). Anterior pig ear skin has been utilized to assess PS accumulation and skin permeability (Reis et al., 2019), while muscle tissues have served as models to evaluate nonspecific thermal injury associated with PDT (Bourre et al., 2008; da S S Campanholi et al., 2018; Dhal et al., 2020; Fujita et al., 2016; González-Delgado et al., 2016; Lim, 2012; Maisch et al., 2010; Sakamoto et al., 2009). Recent advances in tissue engineering have introduced 3D bioprinted constructs and microfluidic organ-on-a-chip systems that enable dynamic simulation of tissue architecture, perfusion, and mechanical forces (Abdelrahim et al., 2022; Flont et al., 2020; Sunil et al., 2022).

In conclusion, non-animal models effectively bridge the gap between animal experiments and clinical trials in PDT research, providing an essential platform for high-throughput screening, mechanistic analysis, and personalized medicine. Future work should focus on technological innovations, such as vascularized organoids and intelligent bioprinting, to enhance the physiological relevance of models and promote interdisciplinary collaboration to establish a multi-level research system from molecules to tissues, thereby accelerating the translation of PDT technologies from laboratory research to clinical application.

Zebrafish for PDT study

Zebrafish models are commonly used as valuable vertebrate models for evaluating the efficacy, safety, and biodistribution of next-generation PS, including NP-based formulations (Figure 4). While mammalian models remain the gold standard for comprehensive pharmacokinetic, pharmacodynamic, and toxicity assessments of novel PS, typically involving serial blood and tissue collection followed by fluorescence imaging, these approaches are expensive, time-consuming, and ethically demanding (Condeelis & Weissleder, 2010). In contrast, zebrafish offer several practical and biological advantages that make them an attractive intermediate model in PDT research. Notably, their optical transparency during early developmental stages enables real-time, non-invasive imaging of PS distribution and light-induced responses at cellular resolution, while their high reproductive capacity, short developmental cycle, and low maintenance costs support the preclinical assessment of biodistribution, tissue penetration, phototoxicity, and therapeutic efficacy of emerging PS candidates in PDT (Table 4). The most widely used laboratory zebrafish strains —Tübingen and AB — exhibit substantial physiological and genetic similarity to humans, including conserved cardiovascular, neurological, and digestive systems, and approximately 70% genetic homology (Goldsmith, 2004). Zebrafish embryogenesis is characterized by rapid development, with major tissues and organs forming within 48–72 h post-fertilization. During this period, embryos transition from the zygotic stage to free-swimming larvae, supported by yolk sac-derived nutrition. By 30 days, larvae undergo metamorphosis into juveniles, with full reproductive maturity typically reached by three months. Among these stages, embryos and larvae are most frequently used in PDT research to evaluate *in vivo* toxicity and therapeutic potential of novel PS. For example, Wang & Qian (2020) introduced a carbazolyl-BODIPY (Cz-BODIPY) PS incorporating an orthogonal donor-acceptor structure and assessed its antitumor efficiency and toxicity in zebrafish embryos and larvae. Similarly, Deiana et al (2023) reported that a heavy-

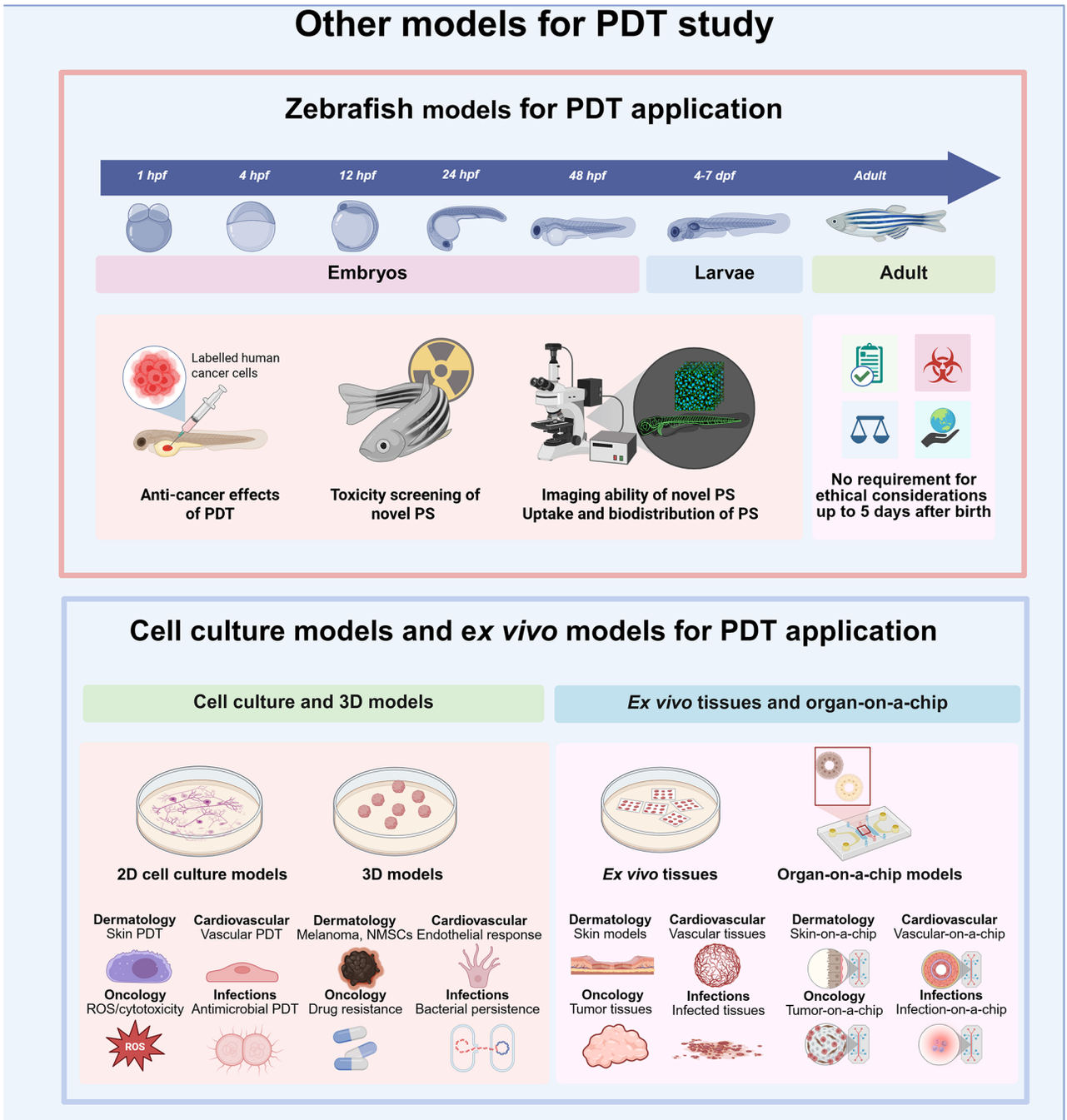

Figure 4 Overview of alternative models used in PDT research, including zebrafish, cell culture, and *ex vivo* models

Zebrafish at various developmental stages are utilized to evaluate the anticancer effects of PDT, screen the toxicity of novel PS, and image PS uptake and biodistribution, with no ethical restrictions up to 5 days. Cell culture and 3D models are widely applied in dermatology, cardiovascular, oncology, and infectious disease research. *Ex vivo* tissues and organ-on-a-chip models also contribute to relevant PDT research in similar fields. HPF: Hours post-fecundation; DPF: Days post-fertilization. Figure created with BioRender.com.

atom-free fluorescent G-quadruplex (G4) DNA-binding PS (DBI) induced cell apoptosis through PDT in zebrafish models. Lillo et al. (2018) analyzed the biodistribution and toxicological profile of amino-functionalized silicon NPs (NH_2SiNPs), employing a range of developmental and physiological endpoints, including lethal concentration 50 (LC50), larval morphology (eye area, rostrocaudal, and spinal length), swimming behavior, and cardiac function. Importantly, zebrafish embryos and larvae offer distinct ethical advantages in experimental design. According to the Council Directive 2010/63/EU on animal experimentation early-stage fish—prior to autonomous feeding —are not classified as protected animals, exempting zebrafish embryos and juveniles (up to 5 days post-fertilization) from standard animal welfare regulations (Hernandez et al., 2018). This exemption is in line with the international '3Rs' principle for the protection and welfare of laboratory animals.

Transparent zebrafish larvae offer a unique *in vivo* platform for real-time visualization of fluorescent PS-NPs (Campbell et al., 2018; Sieber et al., 2017). Stoletov & Klemke (2008) developed folic acid (FA)-ruthenium-complex-silicon NPs, which functioned both as targeted two-photon fluorescence

Table 4 Zebrafish used in PDT research

Photosensitizer	Administration	Developmental stage	Aim of study	References
Organic NPs with aggregation-induced emission	Soaked or i.v. injected	Larvae at 5–7 dpf	• PDT (DLI 48 h, 400–700 nm white light, 135 J/cm^2 or 270 J/cm^2, 150 mW/cm^2) • Uptake/biodistribution of PS • Toxicity	Manghnani et al., 2018
Amino-functionalized silicon NPs (NH_2SiNP)	Soaked	Embryos at 1 hpf Larvae at 4–7 dpf	• Uptake/biodistribution of PS • Toxicity	Lillo et al., 2018
FA-nanoscale gadolinium-porphyrin metal-organic frameworks (FA-NPMOFs)	Soaked	Embryos and larvae at 5 dpf	• PDT (DLI 48 h, 655 nm, 300 mW/cm^2, 10m in) • Uptake/biodistribution of PS • MRI capability • Toxicity	Chen et al., 2018
folate-derived blue-emitting silicon nanoparticles	Soaked	Larvae at 4 dpf	• Toxicity	Calienni et al., 2019
AIE PS dots	Soaked	Embryos and larvae at 5 dpf	• PDT (DLI 24 h, 820 nm, 20 J/cm^2, 6 mW, 5.33 s per scan) • Toxicity	Wang et al., 2019
FA-ruthenium-complex-silicon NPs	Soaked	Embryos	• Imaging capability • Toxicity	Dou et al., 2019
Ce6:$CuFeS_2$@BSA-FA	Soaked	Embryos	• Toxicity	Girma et al., 2019
Silicon quantum dot nanoparticles (SiQDNPs)	Microinjected to embryos	Embryos	• PDT (450 nm, 34 mW/cm^2) • Toxicity	Srivastava et al., 2019
NIR BODIPY PS	Soaked	Embryos	• Imaging capability • Uptake of PS • Toxicity	Liu & Qian, 2024a
Heavy-atom-free BODIPY dendrimer	Soaked	Embryos	• Antimicrobial PDT (DLI 6 h, 488 nm and 800 nm, 60 mW/cm^2, 15 min) • Imaging capability • Toxicity	Wang & Qian, 2024
Casiopeina III-ia (CasIII-ia)-zinc oxide NPs (ZnONPs)	Soaked	Embryos at 48 hpf	• PDT (DLI 1 h, 365 nm, 10 min, combined with chemotherapy) • Imaging capability • Toxicity	Flores-Cruz et al., 2024
carbazolyl-BODIPY (Cz-BODIPY)	Soaked	Larvae at 6 dpf	• PDT (DLI 4 h, 460 nm, 23 mW/cm^2, 15 min) • Uptake/localization of PS	Wang & Qian, 2020
Water-soluble RFP dimers FP_2R"	Soaked	Zebrafish after developed liver tumor	• PDT (DLI 4 h, 460 nm, 23 mW/cm^2, 15 min) • Uptake/localization of PS	Feng & Qian, 2024
AIE Probe	Soaked	Larvae at 3 days	• Imaging ability	Pei et al., 2024
Biopolymeric materials (chitosan, gelatin, and pomegranate peel extract)	Soaked	Zebrafish over 15 days (1.5–2.0 cm long)	• Toxicity	Bertolo et al., 2023
NIR ditriphenylamine Indole-BODIPY	Soaked	Zebrafish	• PDT (DLI 8 h, LED lamp, 90 mW/cm^2, 5min) • Imaging capability • Toxicity	Liu & Qian, 2024b
Periodic mesoporous ionosilica NPs	Microinjected in pericardial cavity	Embryo	• PDT (DLI 6 h, 660 nm, 60 mW/cm^2, 5min) in combination with siRNA therapy	Mezghrani et al., 2023
Heavy-atom-free fluorescent G-quadruplex (G4) DNA-binding PS (DBI)	Soaked	Embryos at 12–24 hpf	• PDT (DLI 24 h, blue-LED, 55.6 mW/cm^2, 5 min)	Deiana et al., 2023
Rhodamine 6G (R6G)-conjugated gold NPs (AuNP)	Soaked	Embryo	• Imaging capability • Toxicity	Pallavi et al., 2023
Terminalia chebula Polyphenol and IR775-loaded Poly (lactic acid) NPs	Soaked	Embryo at 1–2 hpf	• Imaging capability • Uptake of PS	Pebam et al., 2022
NIR-active Porphyrin-decorated lipid microbubbles	Soaked	Larvae	• Toxicity	Guduru et al., 2022
Metalated phthalocyanines and their hydrophilic derivatives	Soaked	Embryo	• Toxicity	Dias et al., 2022
HCPT@NMOFs-RGD NPs	Soaked	Embryos at 1 hpf, larvae at 5 dpf, and 1-month-old juveniles	• Toxicity • Uptake/biodistribution of PS	Shang et al., 2022
Keratin NPs	Microinjection	Zebrafish animals and embryos	• Toxicity • Uptake/biodistribution of PS	Zhang et al., 2021
NIR and lysosomal targeting thiophene-BODIPY	Soaked	Embryos at 24 hpf	• PDT (DLI 24 h, 660 nm, 90 mW/cm^2, 10 min or 30 min) • Toxicity	Bai et al., 2021
Iridium (III) Photocatalysts	Microinjection	GFP transfected Zebrafish (FLK strain) and embryos (AB strain).	• PDT (DLI 4 h, 671 nm, 15 mW/cm^2, 10 min) • Toxicity	Huang et al., 2021
FA-Ce6/DOX/BNPs	Soaked	Embryos at 4 hpf and larvae	• PDT (DLI 12 h, 465 nm, 11.7 J/cm^2) • Toxicity	Lee et al., 2020
BSA-capped gold nanoclusters	Soaked	Embryos at 1 dpf	• Toxicity	Lillo et al., 2020
TLD1433	Soaked; i.v. injection; retro-orbitally injection	Embryos at 2 dpf	• PDT (DLI 1 h, 520 nm, 114 J/cm^2, 21 mW/cm^2, 90 min) repeated four times	Chen et al., 2020

PS: Photosensitizer; NPs: Nanoparticles; i.v. injection: Intravenous injection; DLI: Drug light interval; DPF: Post-fertilization; HPF: Hours post-fecundation; MRI: Magnetic resonance imaging; NIR: Near infrared; FA: Folic acid; AIE: Aggregation-induced emission; DOX: Doxorubicin; Ce6: Chlorin e6; BSA: Bovine serum albumin; RFP: Red fluorescent protein; HCPT: 10-hydroxycamptothecin; NMOFs: Nanoscale zirconium porphyrin metal-organic frameworks; RGD: Arginine-glycine-aspartic acid. If not specified, zebrafish are wild-type AB strain.

imaging probes and photodynamic agents in zebrafish. Additionally, transgenic zebrafish lines, such as FLK strains expressing fluorescent proteins (e.g., GFP, RFP, and mCherry), can be used for *in vivo* imaging of vasculature and tumor microenvironments, further enhancing the utility of zebrafish for PDT evaluation (Huang et al., 2021). Zebrafish also serve as a valuable intermediate model bridging the biological gap between traditional *in vitro* cytotoxicity assays and large animal preclinical models in oncology. Transgenic tumor models can be established by tissue-specific modulation of oncogenes or tumor suppressors (Huiting et al., 2015). For example, the *EGFP:krasV12* inducible model develops early-stage hepatocellular carcinomas upon doxycycline hydrochloride (Dox) administration from 3 to 7 days post-fertilization. This system enables longitudinal assessment of PS biodistribution, fluorescence-based imaging, biosafety, and PDT efficacy in hepatocellular carcinoma (Chen et al., 2018; Manghnani et al., 2018; Shang et al., 2022; Wang et al., 2019). Beyond genetically engineered lines, zebrafish xenografts have emerged as a robust model for cancer research. Small numbers of tumor cells (25–100) can be microinjected into zebrafish organs, as applied in a wide range of malignancies, including gastric, lung, colorectal, glioblastoma, ovarian, prostate, pancreatic, and hematologic cancers. For instance, a zebrafish breast cancer model was established by microinjecting MDA-MB-231 cells into the yolk sac of zebrafish embryos, enabling investigation of the anticancer efficiency of PDT alone or in combination with chemotherapy (Flores-Cruz et al., 2024). Similarly, Chen et al. (2020) evaluated the route-dependent efficacy of TLD1433-mediated PDT by comparing PS administration via immersion, intravenous injection, and retro-orbital injection. Ectopic tumor models were generated by injecting melanoma cells CRMM2 and CRMM1 into the duct of Cuvier, while orthotopic models were developed by periocular implantation to simulate site-specific tumor growth.

In conclusion, zebrafish represent a powerful platform in PDT research due to their high genetic operability, rapid development, and cost-effectiveness. Through zebrafish models, researchers can evaluate the efficacy of PDT alone or in combination with other conventional therapeutic modalities, thereby gaining a deeper understanding of complex mechanisms of tumor immunology.

CONCLUDING REMARKS AND FUTURE OUTLOOKS

This review provides an in-depth discussion of the mechanisms and current development of PDT, as well as the application and importance of different animal models (Figure 5). Due to its minimally invasive nature, low systemic toxicity, and favorable safety profile, PDT has achieved substantial progress in the treatment of cancers, dermatological conditions, and infectious diseases.

The integration of large animal models into PDT research represents a critical translation step for bridging preclinical findings to clinical implementation. Species such as pigs, dogs, and NHPs exhibit anatomical and physiological characteristics that closely recapitulate human biology, thereby enabling more accurate evaluation of PS distribution, optimal light doses, and tissue-specific response and recovery mechanisms. While rodents (e.g., mice and rats) remain indispensable for high-throughput screening and mechanistic studies, their anatomical limitations—specifically thinner skin (approximately 0.2–0.4 mm in mice and 1–2 mm in rats) and loose subcutaneous tissues—allow visible light (630–690 nm) to penetrate several millimeters, making them suitable for superficial tumor or skin lesion studies. However, these anatomical properties are at odds with the reality of human solid tumors (e.g., breast cancer and hepatocellular carcinoma), which are often located in deeper tissues, potentially leading to an overestimation of PDT efficacy in preclinical studies. In contrast, large animal models, such as pigs, possess skin thickness (1.5–3.0 mm) and dermal architecture comparable to that of humans, along with a complex vascular network, offering a more realistic simulation of light attenuation in deeper tissues. Accordingly, porcine models have become the benchmark for studying PDT in dermatological disorders such as actinic keratosis and non-melanoma skin cancers, supporting optimization of PS dose, light fluence, and exposure timing. The rabbit ear chamber model provides a unique window for real-time visualization of PDT-induced vascular dynamics, enabling investigation of microvascular responses and tissue remodeling. Similarly, NHPs, with ocular anatomy and retinal vasculature nearly identical to those of humans, are uniquely suited for investigating PDT in ophthalmic applications, including CNV in AMD. Canine models, particularly those with spontaneous tumors, reflect the genomic heterogeneity and microenvironmental complexity of human gastrointestinal cancers, enabling clinically relevant assessments of PDT alone or in combination with endoscopic interventions. Together, these animal models, selected for their anatomical fidelity, physiological congruence, and disease modeling capacity, can mimic human disease progression and therapeutic responses, ensuring translational relevance.

Despite their advantages, large animal models in PDT research present several inherent challenges. Interspecies physiological and genetic disparities, even among closely related species, can lead to discrepancies in PS pharmacokinetics, tissue oxygenation dynamics, and immune responses. For example, the accelerated metabolic rate observed in pigs compared to humans may reduce PS circulation time, narrowing the therapeutic window and complicating dose-response optimization. Additionally, high maintenance costs, logistical constraints, and ethical considerations, particularly regarding NHPs, limit their accessibility and scalability. Technical challenges also persist. Achieving uniform light dosimetry across heterogeneous tissue types and consistent PS delivery in deep-seated tumors remain considerable obstacles, further underscoring the need for innovative solutions. To enhance the predictive utility of large-animal systems, future studies should prioritize the development of “humanized” models via advanced gene-editing technologies (e.g., CRISPR/Cas9). These modifications could introduce human-specific targets (e.g., immune checkpoints or hypoxia-inducible factors) to enhance biological relevance. Furthermore, anatomical and physiological differences between species directly influence light penetration depth, PS accumulation, and local oxygen availability—factors that are central to PDT efficacy and must be considered in cross-species extrapolation of dosing parameters. Establishing internationally harmonized protocols for PDT parameters, including standardized metrics for light fluence and drug-light intervals, alongside open-access databases for comparative pharmacokinetic and pharmacodynamic data, will be critical for accelerating the clinical translation of PDT.

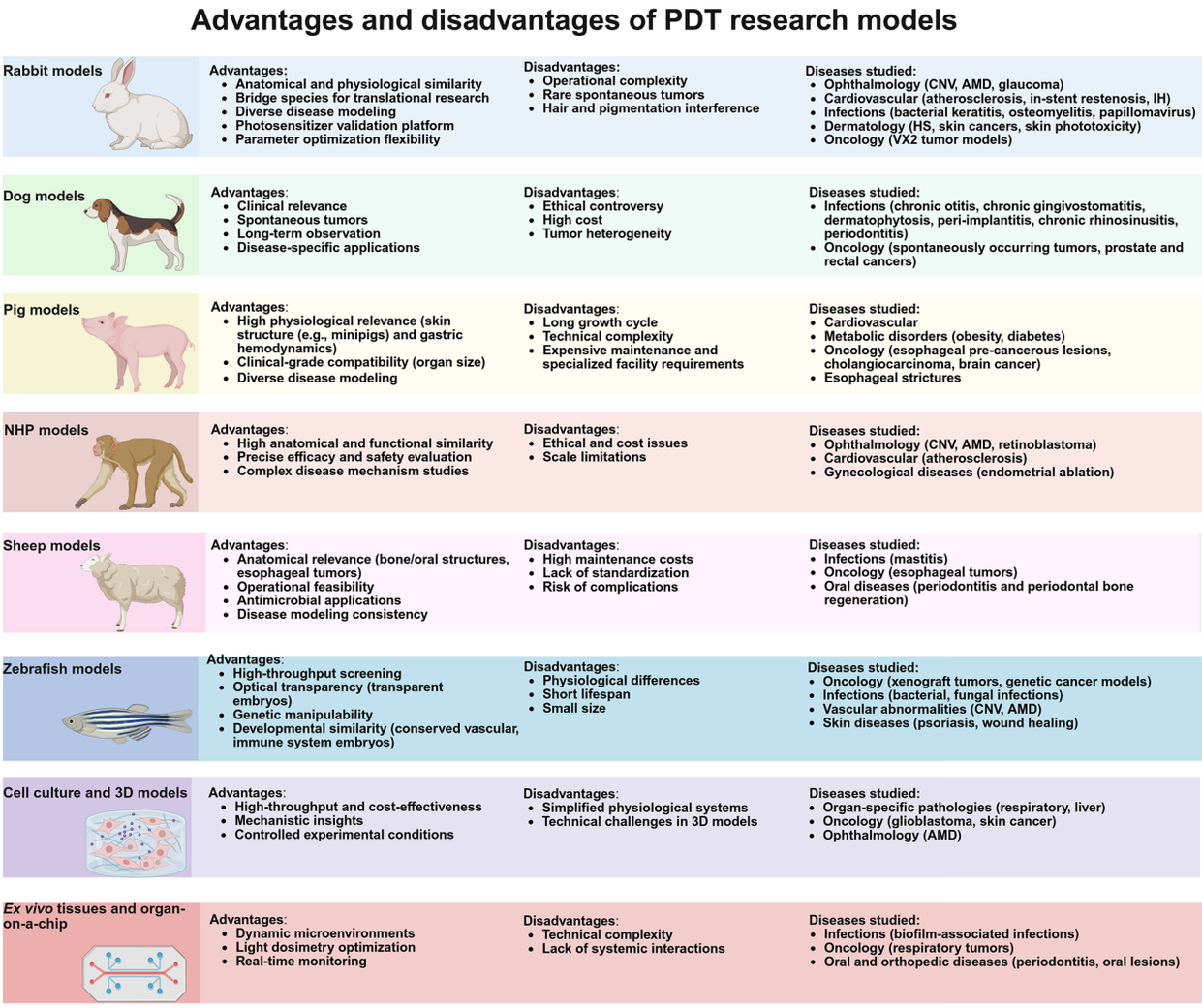

Figure 5 Advantages, disadvantages, and disease applications of *in vivo* and *in vitro* models in PDT research

This figure summarizes key features of various experimental models used in PDT research, including rabbit, dog, pig, NHP, sheep, zebrafish models, as well as cell culture systems, 3D constructs, *ex vivo* tissues, and organ-on-a-chip models. Each model has its own strengths and limitations and is suited to specific disease contexts such as oncology, ophthalmology, and infectious and inflammatory conditions. Figure created with BioRender.com.

In the evolving landscape of PDT research, the future utility of large animal models will increasingly depend on their integration with advanced *in vitro-in vivo* stepwise research systems to balance animal welfare with scientific rigor. A sequential strategy, beginning with high-throughput screening in vascularized organoids or 3D bioprinted tissues, followed by validation in rodent models and targeted large animal models, can streamline preclinical translational workflows while adhering to the principles of the 3Rs. Emerging technologies such as microfluidic organ-on-a-chip platforms, capable of simulating systemic interactions (e.g., PS metabolism in liver compartments and biodistribution in tumor vasculature), may further refine PDT efficacy and toxicity predictions, minimizing the need for exploratory large animal studies. Concurrently, artificial intelligence (AI) tools trained on multimodal datasets, including imaging, multiomics, and clinical outcome records, could be leveraged to identify predictive biomarkers and inform the rational selection of PS, dosing strategies, and animal models. AI-based *in silico* simulations of tissue optics and oxygen diffusion could further refine light dose parameters before *in vivo* testing. Advances in non-invasive imaging modalities also offer substantial potential to reduce animal burden. Techniques such as optoacoustic imaging and Raman spectroscopy enable real-time, longitudinal tracking of PS distribution, ROS generation, and tissue repair without necessitating animal sacrifice, thereby enhancing both scientific rigor and ethical compliance. Furthermore, adoption of the 3Rs principle should be enforced through shared resources, such as the reuse of historical data from previous PDT trials to establish computational models that predict outcomes under new scenarios, thus reducing redundant experimentation.

In conclusion, while large animal models remain critical for validating PDT in anatomically and physiologically relevant systems, their utility must evolve alongside technological and ethical advancements. By harmonizing precision gene-editing, AI-driven analytics, and human-relevant *in vitro* platforms, researchers can maximize the predictive power of these models while minimizing their use. The convergence of these approaches will not only accelerate PDT translation into tailored therapies for complex diseases but also uphold the ethical standards essential for sustainable biomedical

innovation.

COMPETING INTERESTS

The authors declare that they have no competing interests.

AUTHORS' CONTRIBUTIONS

Y.H. and Y.Q.Q. conceptualized the study and drafted the manuscript. H.Z.Z., J.Q.W., S.M. and Y.J.F. reviewed and edited the manuscript. H.Z.Z. and J.Q.W. prepared the figures. Y.H. visualized the figures. D.X.W. and Y.H. supervised the study. Y.H. edited the manuscript. All authors read and approved the final version of the manuscript.

REFERENCES

Abdelrahim AA, Hong S, Song JM. 2022. Integrative *in situ* photodynamic therapy-induced cell death measurement of 3D-bioprinted MCF-7 tumor spheroids. *Analytical Chemistry*, **94**(40): 13936–13943.

Abreu Villela P, de Carvalho de Souza N, Baia JD, et al. 2017. Antimicrobial photodynamic therapy (aPDT) and photobiomodulation (PBM - 660nm) in a dog with chronic gingivostomatitis. *Photodiagnosis and Photodynamic Therapy*, **20**: 273–275.

Aires-Fernandes M, Amantino CF, Do Amaral SR, et al. 2022. Tissue engineering and photodynamic therapy: a new frontier of science for clinical application -an up-to-date review. *Frontiers in Bioengineering and Biotechnology*, **10**: 837693.

Allison BA, Crespo MT, Jain AK, et al. 1997. Delivery of benzoporphyrin derivative, a photosensitizer, into atherosclerotic plaque of Watanabe heritable hyperlipidemic rabbits and balloon-injured New Zealand rabbits. *Photochemistry and Photobiology*, **65**(5): 877–883.

Allison BA, Pritchard PH, Levy JG. 1994. Evidence for low-density lipoprotein receptor-mediated uptake of benzoporphyrin derivative. *British Journal of Cancer*, **69**(5): 833–839.

Allison BA, Waterfield E, Richter AM, et al. 1991. The effects of plasma lipoproteins on in vitro tumor cell killing and in vivo tumor photosensitization with benzoporphyrin derivative. *Photochemistry and Photobiology*, **54**(5): 709–715.

Ansari AA, Lv RC, Gai SL, et al. 2024. ZnO nanostructures – future frontiers in photocatalysis, solar cells, sensing, supercapacitor, fingerprint technologies, toxicity, and clinical diagnostics. *Coordination Chemistry Reviews*, **515**: 215942.

Ansari AA, Parchur AK, Chen GY. 2022. Surface modified lanthanide upconversion nanoparticles for drug delivery, cellular uptake mechanism, and current challenges in NIR-driven therapies. *Coordination Chemistry Reviews*, **457**: 214423.

Arnfield MR, Mathew RP, Tulip J, et al. 1992. Analysis of tissue optical coefficients using an approximate equation valid for comparable absorption and scattering. *Physics in Medicine and Biology*, **37**(6): 1219–1230.

Atayde LM, Cortez PP, Pereira T, et al. 2014. A new sheep model with automatized analysis of biomaterial-induced bone tissue regeneration. *Journal of Materials Science: Materials in Medicine*, **25**(8): 1885–1901.

Bader N, Peschmann C, Kast RE, et al. 2024. Globus lucidus: a porcine study of an intracranial implant designed to deliver closed, repetitive photodynamic and photochemical therapy in glioblastoma. *Photodiagnosis and Photodynamic Therapy*, **46**: 104059.

Bae BC, Yang SG, Jeong S, et al. 2014. Polymeric photosensitizer-embedded self-expanding metal stent for repeatable endoscopic photodynamic therapy of cholangiocarcinoma. *Biomaterials*, **35**(30): 8487–8495.

Bai J, Zhang L, Qian Y. 2021. A near-infrared and lysosomal targeting thiophene-BODIPY photosensitizer: synthesis and its imaging guided photodynamic therapy of cancer cells. *Spectrochimica Acta Part A: Molecular and Biomolecular Spectroscopy*, **252**: 119512.

Berdugo M, Bejjani RA, Valamanesh F, et al. 2008. Evaluation of the new photosensitizer Stakel (WST-11) for photodynamic choroidal vessel occlusion in rabbit and rat eyes. *Investigative Ophthalmology & Visual Science*, **49**(4): 1633–1644.

Bertolo MRV, Dias LD, Lima AR, et al. 2023. Photoantimicrobial chitosan-gelatin-pomegranate peel extract films for strawberries preservation: from microbiological analysis to *in vivo* safety assessment. *International Journal of Biological Macromolecules*, **253**(Pt 5): 127085.

Bogaards A, Varma A, Zhang K, et al. 2005. Fluorescence image-guided brain tumour resection with adjuvant metronomic photodynamic therapy: pre-clinical model and technology development. *Photochemical & Photobiological Sciences*, **4**(5): 438–442.

Bogaards JJP, Bertrand M, Jackson P, et al. 2000. Determining the best animal model for human cytochrome P450 activities: a comparison of mouse, rat, rabbit, dog, micropig, monkey and man. *Xenobiotica*, **30**(12): 1131–1152.

Bonnotte B, Gough M, Phan V, et al. 2003. Intradermal injection, as opposed to subcutaneous injection, enhances immunogenicity and suppresses tumorigenicity of tumor cells. *Cancer Research*, **63**(9): 2145–2149.

Bourre L, Giuntini F, Eggleston IM, et al. 2008. 5-Aminolaevulinic acid peptide prodrugs enhance photosensitization for photodynamic therapy. *Molecular Cancer Therapeutics*, **7**(6): 1720–1729.

Buzzá HH, Holmo Jr D, Stringasci MD, et al. 2019. Photodynamic therapy versus glucose for the treatment of telangiectasia: a randomised controlled study in a rabbit ear model. *European Journal of Vascular and Endovascular Surgery*, **58**(4): 583–591.

Cabral FV, Sellera FP, Ribeiro MS. 2021. Methylene blue-mediated antimicrobial photodynamic therapy for canine dermatophytosis caused by *Microsporum canis*: a successful case report with 6 months follow-up. *Photodiagnosis and Photodynamic Therapy*, **36**: 102602.

Cacaccio JC, Durrani FA, Missert JR, et al. 2022. Photodynamic therapy in combination with doxorubicin is superior to monotherapy for the treatment of lung cancer. *Biomedicines*, **10**(4): 857.

Calienni MN, Lillo CR, Prieto MJ, et al. 2019. Comparative toxicity of PEG and folate-derived blue-emitting silicon nanoparticles: *in vitro* and in vivo studies. *Nanomedicine*, **14**(4): 375–385.

Campbell F, Bos FL, Sieber S, et al. 2018. Directing nanoparticle biodistribution through evasion and exploitation of Stab2-dependent nanoparticle uptake. *ACS Nano*, **12**(3): 2138–2150.

Cao H, Jin Y, Zhao J, et al. 2018. An improved biopsy technique for rabbits with VX2 bone tumors. *Oncology Letters*, **16**(2): 2299–2304.

Castano AP, Mroz P, Hamblin MR. 2006. Photodynamic therapy and anti-tumour immunity. *Nature Reviews Cancer*, **6**(7): 535–545.

Chang SC, Buonaccorsi G, Macrobert A, et al. 1996. Interstitial and transurethral photodynamic therapy of the canine prostate using meso-tetra-(*m*-hydroxyphenyl) chlorin. *International Journal of Cancer*, **67**(4): 555–562.

Chang SC, Chern IF, Hsu YH. 1999. Biological responses of dog prostate and adjacent structures after meso-tetra-(m-hydroxyphenyl) chlorin and aluminum disulfonated phthalocyanine based photodynamic therapy. *Proceedings of the National Science Council, Republic of China. Part B, Life sciences*, **23**(4): 158–166.

Chen DY, Zhang YX, Long W, et al. 2023. Visible light-driven photodynamic therapy for hypertrophic scars with MOF armored microneedles patch. *Frontiers in Chemistry*, **11**: 1128255.

Chen QC, Ramu V, Aydar Y, et al. 2020. TLD1433 Photosensitizer inhibits conjunctival melanoma cells in zebrafish ectopic and orthotopic tumour models. *Cancers*, **12**(3): 587.

Chen Y, Liu W, Shang Y, et al. 2018. Folic acid-nanoscale gadolinium-porphyrin metal-organic frameworks: fluorescence and magnetic resonance dual-modality imaging and photodynamic therapy in hepatocellular

carcinoma. *International Journal of Nanomedicine*, **14**: 57–74.

Cheong KX, Barathi VA, Teo KYC, et al. 2021. Choroidal and retinal changes after systemic adrenaline and photodynamic therapy in non-human primates. *Investigative Ophthalmology & Visual Science*, **62**(3): 25.

Chevalier S, Anidjar M, Scarlata E, et al. 2011. Preclinical study of the novel vascular occluding agent, WST11, for photodynamic therapy of the canine prostate. *The Journal of Urology*, **186**(1): 302–309.

Chevalier S, Cury FL, Scarlata E, et al. 2013. Endoscopic vascular targeted photodynamic therapy with the photosensitizer WST11 for benign prostatic hyperplasia in the preclinical dog model. *The Journal of Urology*, **190**(5): 1946–1953.

Chuang LH, Hwang YS, Wang NK, et al. 2014. The chorioretinal damage caused by different half parameters of photodynamic therapy in rabbits. *Journal of Ocular Pharmacology and Therapeutics*, **30**(8): 642–649.

Ciulla TA, Criswell MH, Snyder WJ, et al. 2005. Photodynamic therapy with PhotoPoint photosensitiser MV6401, indium chloride methyl pyropheophorbide, achieves selective closure of rat corneal neovascularisation and rabbit choriocapillaris. *British Journal of Ophthalmology*, **89**(1): 113–119.

Condeelis J, Weissleder R. 2010. *In vivo* imaging in cancer. *Cold Spring Harbor Perspectives in Biology*, **2**(12): a003848.

Costa RA, Farah ME, Freymüller E, et al. 2001. Choriocapillaris photodynamic therapy using indocyanine green. *American Journal of Ophthalmology*, **132**(4): 557–565.

Criswell MH, Ciulla TA, Lowseth LA, et al. 2005. Anastomotic vessels remain viable after photodynamic therapy in primate models of choroidal neovascularization. *Investigative Ophthalmology & Visual Science*, **46**(6): 2168–2174.

da S S Campanholi K, Braga G, Da Silva JB, et al. 2018. Biomedical platform development of a chlorophyll-based extract for topic photodynamic therapy: mechanical and spectroscopic properties. *Langmuir*, **34**(28): 8230–8244.

Daniell MD, Hill JS. 1991. A history of photodynamic therapy. *Australian and New Zealand Journal of Surgery*, **61**(5): 340–348.

De Nardi AB, De Oliveira Massoco Salles Gomes C, Fonseca-Alves CE, et al. 2023. Diagnosis, prognosis, and treatment of canine hemangiosarcoma: a review based on a consensus organized by the Brazilian association of veterinary oncology, ABROVET. *Cancers*, **15**(7): 2025.

De Oliveira RR, Novaes Jr AB, Garlet GP, et al. 2011. The effect of a single episode of antimicrobial photodynamic therapy in the treatment of experimental periodontitis. Microbiological profile and cytokine pattern in the dog mandible. *Lasers in Medical Science*, **26**(3): 359–367.

Deiana M, Andrés Castán JM, Josse P, et al. 2023. A new G-quadruplex-specific photosensitizer inducing genome instability in cancer cells by triggering oxidative DNA damage and impeding replication fork progression. *Nucleic Acids Research*, **51**(12): 6264–6285.

Dhal S, Verma P, Mishra M, et al. 2020. Oleogel-mediated transdermal delivery of white emitting $NaYF_4$ conjugated with Rose Bengal for the generation of reactive oxygen species through NIR-upconversion. *Colloids and Surfaces B: Biointerfaces*, **190**: 110945.

Dias LM, De Keijzer MJ, Ernst D, et al. 2022. Metallated phthalocyanines and their hydrophilic derivatives for multi-targeted oncological photodynamic therapy. *Journal of Photochemistry and Photobiology B: Biology*, **234**: 112500.

Dinchuk J, Hart J, Gonzalez G, et al. 1995. Remodelling of lipoproteins in transgenic mice expressing human cholesteryl ester transfer protein. *Biochimica et Biophysica Acta (BBA) - Lipids and Lipid Metabolism*, **1255**(3): 301–310.

Dou YK, Shang Y, He XW, et al. 2019. Preparation of a ruthenium-complex-functionalized two-photon-excited red fluorescence silicon nanoparticle composite for targeted fluorescence imaging and photodynamic therapy *in vitro*. *ACS Applied Materials & Interfaces*, **11**(15): 13954–13963.

Du KL, Mick R, Busch TM, et al. 2006. Preliminary results of interstitial motexafin lutetium-mediated PDT for prostate cancer. *Lasers in Surgery and Medicine*, **38**(5): 427–434.

Du W, Lee YC, Wang TF, et al. 2021. Dose-related structural effects of photodynamic therapy on rabbit choroidal structure. *Ophthalmic Research*, **64**(6): 1037–1047.

Durrani FA, Cacaccio J, Turowski SG, et al. 2023. Photobac derived from bacteriochlorophyll-a shows potential for treating brain tumor in animal models by photodynamic therapy with desired pharmacokinetics and limited toxicity in rats and dogs. *Biomedicine & Pharmacotherapy*, **168**: 115731.

Eifler AC, Lewandowski RJ, Virmani S, et al. 2009. Development of a VX2 pancreatic cancer model in rabbits: a pilot study. *Journal of Vascular and Interventional Radiology*, **20**(8): 1075–1082.

Eldar M, Yerushalmi Y, Kessler E, et al. 1990. Preferential uptake of a water-soluble phthalocyanine by atherosclerotic plaques in rabbits. *Atherosclerosis*, **84**(2-3): 135–139.

Fan DH, Cao YK, Cao MQ, et al. 2023. Nanomedicine in cancer therapy. *Signal Transduction and Targeted Therapy*, **8**(1): 293.

Fan JL, Kitajima S, Watanabe T, et al. 2015. Rabbit models for the study of human atherosclerosis: from pathophysiological mechanisms to translational medicine. *Pharmacology & Therapeutics*, **146**: 104–119.

Feng W, Qian Y. 2024. Water-soluble red fluorescent protein dimers for hypoxic two-photon photodynamic therapy. *Journal of Materials Chemistry B*, **12**(9): 2413–2424.

Flont M, Jastrzebska E, Brzózka Z. 2020. A multilayered cancer-on-a-chip model to analyze the effectiveness of new-generation photosensitizers. *Analyst*, **145**(21): 6937–6947.

Flores-Cruz RD, Espinoza-Guillen A, Resendiz-Acevedo K, et al. 2024. Doble synergetic anticancer activity through a combined chemo-photodynamic therapy and bioimaging of a novel Cas-ZnONPs all-in-one system. *Journal of Inorganic Biochemistry*, **258**: 112623.

Foster JR, Mowat V, Singh BP, et al. 2022. Animal models in toxicologic research: dog. *In*: Haschek WM, Rousseaux CG, Wallig MA, et al. Haschek and Rousseaux's Handbook of Toxicologic Pathology. Amsterdam: Elsevier, 721–750.

Framme C, Flucke B, Birngruber R. 2006a. Comparison of reduced and standard light application in photodynamic therapy of the eye in two rabbit models. *Graefe's Archive for Clinical and Experimental Ophthalmology*, **244**(7): 773–781.

Framme C, Sachs HG, Flucke B, et al. 2006b. Evaluation of the new photosensitizer Tookad (WST09) for photodynamic vessel occlusion of the choroidal tissue in rabbits. *Investigative Ophthalmology & Visual Science*, **47**(12): 5437–5446.

Fujita AKL, Rodrigues PGS, Requena MB, et al. 2016. Fluorescence evaluations for porphyrin formation during topical PDT using ALA and methyl-ALA mixtures in pig skin models. *Photodiagnosis and Photodynamic Therapy*, **15**: 236–244.

Furuse K, Fukuoka M, Kato H, et al. 1993. A prospective phase II study on photodynamic therapy with photofrin II for centrally located early-stage lung cancer. The Japan Lung Cancer Photodynamic Therapy Study Group. *Journal of Clinical Oncology*, **11**(10): 1852–1857.

Gallardo D, Pena RN, Amills M, et al. 2008. Mapping of quantitative trait loci for cholesterol, LDL, HDL, and triglyceride serum concentrations in pigs. *Physiological Genomics*, **35**(3): 199–209.

Gao H, Shi L, Yin HJ, et al. 2016. Evaluation of the effect of photodynamic therapy with hematoporphyrin monomethyl ether on VX2 tumors implanted in the rectal submucosa of rabbits. *Journal of Photochemistry and Photobiology B: Biology*, **163**: 162–169.

Girma WM, Dehvari K, Ling YC, et al. 2019. Albumin-functionalized

$CuFeS_2$/photosensitizer nanohybrid for single-laser-induced folate receptor-targeted photothermal and photodynamic therapy. *Materials Science and Engineering: C*, **101**: 179–189.

Gohto Y, Obana A, Kanai M, et al. 2001. Treatment parameters for selective occlusion of experimental corneal neovascularization by photodynamic therapy using a water soluble photosensitizer, ATX-S10(Na). *Experimental Eye Research*, **72**(1): 13–22.

Gohto Y, Obana A, Kaneda K, et al. 2000. Accumulation of photosensitizer ATX-S10 (Na) in experimental corneal neovascularization. *Japanese Journal of Ophthalmology*, **44**(4): 348–353.

Goldsmith P. 2004. Zebrafish as a pharmacological tool: the how, why and when. *Current Opinion in Pharmacology*, **4**(5): 504–512.

Goldstein JL, Brown MS. 2009. The LDL receptor. *Arteriosclerosis, Thrombosis, and Vascular Biology*, **29**(4): 431–438.

Gomer CJ, Jester JV, Razum NJ, et al. 1985. Photodynamic therapy of intraocular tumors: examination of hematoporphyrin derivative distribution and long-term damage in rabbit ocular tissue. *Cancer Research*, **45**(8): 3718–3725.

González-Delgado JA, Castro PM, Machado A, et al. 2016. Hydrogels containing porphyrin-loaded nanoparticles for topical photodynamic applications. *International Journal of Pharmaceutics*, **510**(1): 221–231.

Gonzalez VH, Hu LK, Theodossiadis PG, et al. 1995. Photodynamic therapy of pigmented choroidal melanomas. *Investigative Ophthalmology & Visual Science*, **36**(5): 871–878.

Guduru ATKVVNSK, Manav N, Mansuri A, et al. 2022. NIR-active porphyrin-decorated lipid microbubbles for enhanced therapeutic activity enabled by photodynamic effect and ultrasound in 3D tumor models of breast cancer cell line and zebrafish larvae. *ACS Applied Bio Materials*, **5**(9): 4270–4283.

Guidi EEA, Vercelli A, Corona A, et al. 2021. A case of drug-resistant staphylococcal para-aural abscess treated with photodynamic therapy in a West Highland White Terrier presenting with chronic otitis and craniomandibular osteopathy. *Photodiagnosis and Photodynamic Therapy*, **35**: 102424.

Gunti S, Hoke ATK, Vu KP, et al. 2021. Organoid and spheroid tumor models: techniques and applications. *Cancers*, **13**(4): 874.

Gutierrez K, Dicks N, Glanzner WG, et al. 2015. Efficacy of the porcine species in biomedical research. *Frontiers in Genetics*, **6**: 293.

Haimovici R, Ciulla TA, Miller JW, et al. 2002. Localization of rose bengal, aluminum phthalocyanine tetrasulfonate, and chlorin e6 in the rabbit eye. *Retina*, **22**(1): 65–74.

Haitina T, Fredriksson R, Foord SM, et al. 2009. The G protein-coupled receptor subset of the dog genome is more similar to that in humans than rodents. *BMC Genomics*, **10**(1): 24.

Handal JA, Schulz JF, Florez GB, et al. 2013. Creation of rabbit bone and soft tissue tumor using cultured VX_2 cells. *The Journal of Surgical Research*, **179**(1): e127–e132.

Hanisch UK, Kettenmann H. 2007. Microglia: active sensor and versatile effector cells in the normal and pathologic brain. *Nature Neuroscience*, **10**(11): 1387–1394.

Hao Y, Chung CK, Gu ZL, et al. 2022a. Combinatorial therapeutic approaches of photodynamic therapy and immune checkpoint blockade for colon cancer treatment. *Molecular Biomedicine*, **3**(1): 26.

Hao Y, Chung CK, Yu ZF, et al. 2022b. Combinatorial therapeutic approaches with nanomaterial-based photodynamic cancer therapy. *Pharmaceutics*, **14**(1): 120.

Hao Y, Ma S, Gu ZL, et al. 2023b. Combination of photodynamic therapy and stimulator of interferon genes (STING) agonist inhibits colorectal tumor growth and recurrence. *Cancer Communications*, **43**(4): 513–518.

Heckenkamp J, Mellander S, Fogelstrand P, et al. 2007. Photodynamic therapy reduces intimal hyperplasia in prosthetic vascular bypass grafts in a pig model. *European Journal of Vascular and Endovascular Surgery*, **34**(3): 333–339.

Hernandez RE, Galitan L, Cameron J, et al. 2018. Delay of initial feeding of zebrafish larvae until 8 days postfertilization has no impact on survival or growth through the juvenile stage. *Zebrafish*, **15**(5): 515–518.

Hickey AR, Wenger TL, Carpenter VP, et al. 1991. Digoxin Immune Fab therapy in the management of digitalis intoxication: safety and efficacy results of an observational surveillance study. *Journal of the American College of Cardiology*, **17**(3): 590–598.

Hill RA, Esterowitz T, Ryan J, et al. 1995. Photodynamic laser cyclodestruction with chloroaluminum sulfonated phthalocyanine (CASPc) or Photofrin (PII) vs. Nd: YAG laser cyclodestruction in a pigmented rabbit model. *Lasers in Surgery and Medicine*, **17**(2): 166–171.

Hirsch HA, Iliopoulos D, Joshi A, et al. 2010. A transcriptional signature and common gene networks link cancer with lipid metabolism and diverse human diseases. *Cancer Cell*, **17**(4): 348–361.

Holzer MP, Solomon KD, Vroman DT, et al. 2003. Photodynamic therapy with verteporfin in a rabbit model of corneal neovascularization. *Investigative Ophthalmology & Visual Science*, **44**(7): 2954–2958.

Huang C, Liang C, Sadhukhan T, et al. 2021. *In-vitro* and *in-vivo* photocatalytic cancer therapy with biocompatible iridium(III) photocatalysts. *Angewandte Chemie International Edition*, **60**(17): 9474–9479.

Huang LH, Elvington A, Randolph GJ. 2015. The role of the lymphatic system in cholesterol transport. *Frontiers in Pharmacology*, **6**: 182.

Huiting LN, Laroche F, Feng H. 2015. The zebrafish as a tool to cancer drug discovery. *Austin Journal of Pharmacology and Therapeutics*, **3**(2): 1069.

Husain D, Kim I, Gauthier D, et al. 2005. Safety and efficacy of intravitreal injection of ranibizumab in combination with verteporfin PDT on experimental choroidal neovascularization in the monkey. *Archives of Ophthalmology*, **123**(4): 509–516.

Husain D, Kramer M, Kenny AG, et al. 1999. Effects of photodynamic therapy using verteporfin on experimental choroidal neovascularization and normal retina and choroid up to 7 weeks after treatment. *Investigative Ophthalmology & Visual Science*, **40**(10): 2322–2331.

Husain D, Miller JW, Kenney AG, et al. 1997. Photodynamic therapy and digital angiography of experimental iris neovascularization using liposomal benzoporphyrin derivative. *Ophthalmology*, **104**(8): 1242–1250.

Husain D, Miller JW, Michaud N, et al. 1996. Intravenous infusion of liposomal benzoporphyrin derivative for photodynamic therapy of experimental choroidal neovascularization. *Archives of Ophthalmology*, **114**(8): 978–985.

Hytönen MK, Lohi H. 2016. Canine models of human rare disorders. *Rare Diseases*, **4**(1): e1241362.

Jacobs TM, Rosen GM. 2000. Photodynamic therapy as a treatment for esophageal squamous cell carcinoma in a dog. *Journal of the American Animal Hospital Association*, **36**(3): 257–261.

Jenkins MP, Buonaccorsi G, Macrobert A, et al. 1998. Intra-arterial photodynamic therapy using 5-ALA in a swine model. *European Journal of Vascular and Endovascular Surgery*, **16**(4): 284–291.

Jones LR, Preyer NW, Wolfsen HC, et al. 2009. Monte Carlo model of stricture formation in photodynamic therapy of normal pig esophagus. *Photochemistry and Photobiology*, **85**(1): 341–346.

Joudeh N, Linke D. 2022. Nanoparticle classification, physicochemical properties, characterization, and applications: a comprehensive review for biologists. *Journal of Nanobiotechnology*, **20**(1): 262.

Kaabia Z, Poirier J, Moughaizel M, et al. 2018. Plasma lipidomic analysis reveals strong similarities between lipid fingerprints in human, hamster and mouse compared to other animal species. *Scientific Reports*, **8**(1): 15893.

Kessel D. 1986. Porphyrin-lipoprotein association as a factor in porphyrin localization. *Cancer Letters*, **33**(2): 183–188.

Kessels J, Kreukels H, Nelemans PJ, et al. 2018. Treatment of superficial basal cell carcinoma by topical photodynamic therapy with fractionated 5-aminolaevulinic acid 20% vs. two-stage topical methyl aminolaevulinate: results of a randomized controlled trial. *British Journal of Dermatology*, **178**(5): 1056–1063.

Khan I, Saeed K, Khan I. 2019. Nanoparticles: properties, applications and toxicities. *Arabian Journal of Chemistry*, **12**(7): 908–931.

Kim IK, Husain D, Michaud N, et al. 2006. Effect of intravitreal injection of ranibizumab in combination with verteporfin PDT on normal primate retina and choroid. *Investigative Ophthalmology & Visual Science*, **47**(1): 357–363.

Kim JW, Jacobsen B, Zolfaghari E, et al. 2017. Rabbit model of ocular indirect photodynamic therapy using a retinoblastoma xenograft. *Graefe's Archive for Clinical and Experimental Ophthalmology*, **255**(12): 2363–2373.

Kim JW, Lee S, Ryu DS, et al. 2023. Photoactive intragastric satiety-inducing device using polymeric photosensitizers for minimally invasive weight loss treatment. *Biomaterials*, **299**: 122159.

Kim RY, Hu LK, Foster BS, et al. 1996. Photodynamic therapy of pigmented choroidal melanomas of greater than 3–mm thickness. *Ophthalmology*, **103**(12): 2029–2036.

Kimm SY, Tarin TV, Monette S, et al. 2016. Nonthermal ablation by using intravascular oxygen radical generation with WST11: dynamic tissue effects and implications for focal therapy. *Radiology*, **281**(1): 109–118.

Koh HJ, Kang SJ, Lim SJ, et al. 2002. The effect of photodynamic therapy with rose bengal on posterior capsule opacification in rabbit eyes. *Ophthalmic Research*, **34**(3): 107–112.

Konan YN, Gurny R, Allémann E. 2002. State of the art in the delivery of photosensitizers for photodynamic therapy. *Journal of Photochemistry and Photobiology B: Biology*, **66**(2): 89–106.

Kranz S, Heyder M, Rabe U, et al. 2023. Osseointegration of photodynamic active biomaterials for bone regeneration in an animal bone model over a period of 12 months. *Dental Materials*, **39**(11): 977–985.

Kumar D, Tahsini L, De Visser SP, et al. 2009. Effect of porphyrin ligands on the regioselective dehydrogenation versus epoxidation of olefins by oxoiron(IV) mimics of cytochrome P450. *The Journal of Physical Chemistry A*, **113**(43): 11713–11722.

Kurano M, Hara M, Ikeda H, et al. 2017. Involvement of CETP (cholesteryl ester transfer protein) in the shift of sphingosine-1-phosphate among lipoproteins and in the modulation of its functions. *Arteriosclerosis, Thrombosis, and Vascular Biology*, **37**(3): 506–514.

Kwiatkowski S, Knap B, Przystupski D, et al. 2018. Photodynamic therapy-mechanisms, photosensitizers and combinations. *Biomedicine & Pharmacotherapy*, **106**: 1098–1107.

Kwon OC, Yoon HJ, Kim KH, et al. 2008. Fluorescence kinetics of protoporphyrin–IX induced from 5-ALA compounds in rabbit postballoon injury model for ALA-photoangioplasty. *Photochemistry and Photobiology*, **84**(5): 1209–1214.

Lara P, Huis in 't Veld RV, Jorquera-Cordero C, et al. 2021. Zinc-phthalocyanine-loaded extracellular vesicles increase efficacy and selectivity of photodynamic therapy in co–culture and preclinical models of colon cancer. *Pharmaceutics*, **13**(10): 1547.

Lee H, Kim S, Oh C, et al. 2020. Folic acid-modified bovine serum albumin nanoparticles with doxorubicin and chlorin e6 for effective combinational chemo-photodynamic therapy. *Materials Science and Engineering: C*, **117**: 111343.

Li BH, Lin L. 2022. Internal light source for deep photodynamic therapy. *Light*: *Science & Applications*, **11**(1): 85.

Li CZ, Cheng LF, Wang ZQ, et al. 2003. Photodynamic therapy of esophageal varices: experimental studies in animal veins, and first clinical cases. *Endoscopy*, **35**(12): 1043–1048.

Li CZ, Cheng LF, Wang ZQ, et al. 2009. Attempt of photodynamic therapy on esophageal varices. *Lasers in Medical Science*, **24**(2): 167–171.

Li JL, Guo ZF, Wu JG. 2024. Investigation into safflower injection as a prophylactic treatment for retinal vein occlusion in a rabbit model. *Scientific Reports*, **14**(1): 8048.

Lillo CR, Calienni MN, Rivas Aiello B, et al. 2020. BSA–capped gold nanoclusters as potential theragnostic for skin diseases: photoactivation, skin penetration, *in vitro*, and *in vivo* toxicity. *Materials Science and Engineering: C*, **112**: 110891.

Lillo CR, Natalia Calienni M, Gorojod RM, et al. 2018. Toward biomedical application of amino–functionalized silicon nanoparticles. *Nanomedicine*, **13**(11): 1349–1370.

Lim HS. 2012. Reduction of thermal damage in photodynamic therapy by laser irradiation techniques. *Journal of Biomedical Optics*, **17**(12): 128001.

Lin SC, Lin CP, Feld JR, et al. 1994. The photodynamic occlusion of choroidal vessels using benzoporphyrin derivative. *Current Eye Research*, **13**(7): 513–522.

Liu JB, Miller LS, Goldberg BB, et al. 1992. Transnasal US of the esophagus: preliminary morphologic and function studies. *Radiology*, **184**(3): 721–727.

Liu RB, Qian Y. 2024a. Near-infrared BODIPY photosensitizers for two-photon excited singlet oxygen generation and tumor cell photodynamic therapy. *Organic & Biomolecular Chemistry*, **22**(27): 5569–5577.

Liu RB, Qian Y. 2024b. NIR ditriphenylamine Indole-BODIPY photosensitizer: synthesis, photodynamic therapy in A549 cells and two-photon fluorescence imaging in zebrafish. *Spectrochimica Acta Part A: Molecular and Biomolecular Spectroscopy*, **304**: 123387.

Lofgren LA, Ronn AM, Nouri M, et al. 1995. Efficacy of intravenous delta-aminolaevulinic acid photodynamic therapy on rabbit papillomas. *British Journal of Cancer*, **72**(4): 857–864.

Lucky SS, Soo KC, Zhang Y. 2015. Nanoparticles in photodynamic therapy. *Chemical Reviews*, **115**(4): 1990–2042.

Lucroy MD, Ridgway TD, Peavy GM, et al. 2003. Preclinical evaluation of 5-aminolevulinic acid–based photodynamic therapy for canine transitional cell carcinoma. *Veterinary and Comparative Oncology*, **1**(2): 76–85.

Ma CQ, Xie JY, Luo CH, et al. 2019. OxLDL promotes lymphangiogenesis and lymphatic metastasis in gastric cancer by upregulating VEGF-C expression and secretion. *International Journal of Oncology*, **54**(2): 572–584.

Maas AL, Carter SL, Wileyto EP, et al. 2012. Tumor vascular microenvironment determines responsiveness to photodynamic therapy. *Cancer Research*, **72**(8): 2079–2088.

MacEwen EG. 1990. Spontaneous tumors in dogs and cats: models for the study of cancer biology and treatment. *Cancer and Metastasis Reviews*, **9**(2): 125–136.

Madi M, Alagl AS. 2018. The effect of different implant surfaces and photodynamic therapy on periodontopathic bacteria using TaqMan PCR assay following peri-implantitis treatment in dog model. *BioMed Research International*, **2018**: 7570105.

Mahmoudi H, Bahador A, Pourhajibagher M, et al. 2018. Antimicrobial photodynamic therapy: an effective alternative approach to control bacterial infections. *Journal of Lasers in Medical Sciences*, **9**(3): 154–160.

Maisch T, Santarelli F, Schreml S, et al. 2010. Fluorescence induction of protoporphyrin IX by a new 5–aminolevulinic acid nanoemulsion used for photodynamic therapy in a full-thickness *ex vivo* skin model. *Experimental Dermatology*, **19**(8): e302–305.

Mallas E, Karamanolis G, Zissis M, et al. 2004. Photodynamic therapy in normal pig stomach: protective effect of octreotide. *Endoscopy*, **36**(10): 893–897.

Manghnani PN, Wu WB, Xu SD, et al. 2018. Visualizing photodynamic therapy in transgenic zebrafish using organic nanoparticles with aggregation-induced emission. *Nano-Micro Letters*, **10**(4): 61.

Mansoori B, Mohammadi A, Amin Doustvandi M, et al. 2019. Photodynamic therapy for cancer: role of natural products. *Photodiagnosis and Photodynamic Therapy*, **26**: 395–404.

Mapara M, Thomas BS, Bhat KM. 2012. Rabbit as an animal model for experimental research. *Dental Research Journal*, **9**(1): 111–118.

Marijnissen JPA, Baas P, Beek JF, et al. 1993. Pilot study on light dosimetry for endobronchial photodynamic therapy. *Photochemistry and Photobiology*, **58**(1): 92–99.

Marques PE, Nyegaard S, Collins RF, et al. 2019. Multimerization and retention of the scavenger receptor SR–B1 in the plasma membrane. *Developmental Cell*, **50**(3): 283–295. e5.

Martinez MN, Mochel JP, Neuhoff S, et al. 2021. Comparison of canine and human physiological factors: understanding interspecies differences that impact drug pharmacokinetics. *The AAPS Journal*, **23**(3): 59.

Mauro N, Utzeri MA, Varvarà P, et al. 2021. Functionalization of metal and carbon nanoparticles with potential in cancer theranostics. *Molecules*, **26**(11): 3085.

Mayo GL, Melendez RF, Kumar N, et al. 2003. Antibody-targeted photodynamic therapy. *American Journal of Ophthalmology*, **136**(6): 1151–1152.

Mezghrani B, Ali LMA, Cubedo N, et al. 2023. Periodic mesoporous ionosilica nanoparticles for dual cancer therapy: two–photon excitation siRNA gene silencing in cells and photodynamic therapy in zebrafish embryos. *International Journal of Pharmaceutics*, **641**: 123083.

Miller H, Miller B. 1993. Photodynamic therapy of subretinal neovascularization in the monkey eye. *Archives of Ophthalmology*, **111**(6): 855–860.

Miller JW. 2008. Higher irradiance and photodynamic therapy for age–related macular degeneration (an AOS thesis). *Transactions of the American Ophthalmological Society*, **106**: 357–382.

Mohammad-Hadi L, Macrobert AJ, Loizidou M, et al. 2018. Photodynamic therapy in 3D cancer models and the utilisation of nanodelivery systems. *Nanoscale*, **10**(4): 1570–1581.

Monstrey S, Middelkoop E, Vranckx JJ, et al. 2014. Updated scar management practical guidelines: non–invasive and invasive measures. *Journal of Plastic, Reconstructive & Aesthetic Surgery*, **67**(8): 1017–1025.

Morris DE, Wu L, Zhao LL, et al. 1997. Acute and chronic animal models for excessive dermal scarring: quantitative studies. *Plastic and Reconstructive Surgery*, **100**(3): 674–681.

Moshfeghi D, Peyman GA, Kazi AA, et al. 1999. Fluorescence properties of a hydrophilic sensitizer in pigmented rats, rabbits, and monkeys. *Ophthalmic Surgery, Lasers and Imaging Retina*, **30**(9): 750–753.

Muhanna N, Chan HHL, Townson JL, et al. 2020. Photodynamic therapy enables tumor–specific ablation in preclinical models of thyroid cancer. *Endocrine-Related Cancer*, **27**(2): 41–53.

Muhanna N, Cui LY, Chan H, et al. 2016. Multimodal image-guided surgical and photodynamic interventions in head and neck cancer: from primary tumor to metastatic drainage. *Clinical Cancer Research*, **22**(4): 961–970.

Murrer LHP, Hebeda KM, Marijnissen JPA, et al. 1999. Short- and long-term normal tissue damage with photodynamic therapy in pig trachea: a fluence–response pilot study comparing Photofrin and mTHPC. *British Journal of Cancer*, **80**(5-6): 744–755.

Nagae T, Aizawa K, Uchimura N, et al. 2001. Endovascular photodynamic therapy using mono–L–aspartyl–chlorin e6 to inhibit Intimal hyperplasia in balloon-injured rabbit arteries. *Lasers in Surgery and Medicine*, **28**(4): 381–388.

Nagamine N, Ido K, Saihuku K, et al. 2002. Photodynamic effects on rabbit auricular veins after photosensitization with porfimer sodium: implications of the results with respect to the treatment of esophageal varices with photodynamic therapy. *Gastrointestinal Endoscopy*, **55**(3): 420–424.

Nakagishi Y, Morimoto Y, Fujita M, et al. 2005. Rabbit model of airway stenosis induced by scraping of the tracheal mucosa. *The Laryngoscope*, **115**(6): 1087–1092.

Nakagishi Y, Morimoto Y, Fujita M, et al. 2008. Photodynamic therapy for airway stenosis in rabbit models. *Chest*, **133**(1): 123–130.

Nakashima–Nakasuga C, Hazama S, Suzuki N, et al. 2020. Serum LOX-1 is a novel prognostic biomarker of colorectal cancer. *International Journal of Clinical Oncology*, **25**(7): 1308–1317.

Nath S, Moore K. 2019. Photodynamic therapy in a 3D model of ovarian cancer. *Bio-protocol*, **9**(15): e3314.

Nuss KM, Auer JA, Boos A, et al. 2006. An animal model in sheep for biocompatibility testing of biomaterials in cancellous bones. *BMC Musculoskeletal Disorders*, **7**: 67.

Obana A, Gohto Y, Kanai M, et al. 2000. Selective photodynamic effects of the new photosensitizer ATX–S10(Na) on choroidal neovascularization in monkeys. *Archives of Ophthalmology*, **118**(5): 650–658.

Obana A, Gohto Y, Kaneda K, et al. 2001. PDT to monkey CNV with ATX–S10(Na): inappropriateness of early laser irradiation for selective occlusion. *Investigative Ophthalmology & Visual Science*, **42**(11): 2639–2645.

O'Connor AE, Gallagher WM, Byrne AT. 2009. Porphyrin and nonporphyrin photosensitizers in oncology: preclinical and clinical advances in photodynamic therapy. *Photochemistry and Photobiology*, **85**(5): 1053–1074.

Ohnishi Y, Yoshitomi T, Murata T, et al. 2002. Electron microscopic study of monkey retina after photodynamic treatment. *Medical Electron Microscopy*, **35**(1): 46–52.

Ohtani K, Usuda J, Maehara S, et al. 2020. A combination therapy of photodynamic therapy (PDT) and airway stent placement using a transparent silicone stent. *Lasers in Medical Science*, **35**(5): 1035–1040.

Olofsson SO, Borèn J. 2005. Apolipoprotein B: a clinically important apolipoprotein which assembles atherogenic lipoproteins and promotes the development of atherosclerosis. *Journal of Internal Medicine*, **258**(5): 395–410.

Osaki T, Hibino S, Murahata Y, et al. 2023. Vascular-targeted photodynamic therapy with glucose–conjugated chlorin e6 for dogs with spontaneously occurring tumours. *Veterinary Medicine and Science*, **9**(6): 2534–2541.

Osaki T, Takagi S, Hoshino Y, et al. 2012. Temporary regression of locally invasive polypoid rhinosinusitis in a dog after photodynamic therapy. *Australian Veterinary Journal*, **90**(11): 442–447.

Osaki T, Yokoe I, Sunden Y, et al. 2019. Efficacy of 5-aminolevulinic acid in photodynamic detection and photodynamic therapy in veterinary medicine. *Cancers (Basel)*, **11**(4): 495.

Pallavi P, Harini K, Crowder S, et al. 2023. Rhodamine-conjugated anti–stokes gold nanoparticles with higher ROS quantum yield as theranostic probe to arrest cancer and MDR Bacteria. *Applied Biochemistry and Biotechnology*, **195**(11): 6979–6993.

Park JH, Kim JW, Ryu DS, et al. 2024. Repeated photodynamic therapy using a chlorin e6-embedded device to prolong the therapeutic effects on obesity. *Obesity*, **32**(5): 911–922.

Pascale F, Pelage JP, Wassef M, et al. 2022. Rabbit VX2 liver tumor model: a review of clinical, biology, histology, and tumor microenvironment characteristics. *Frontiers in Oncology*, **12**: 871829.

Payne JT, Mccaw DL, Casteel SW, et al. 1996. Pharmacokinetics of pyropheophorbide-a-hexyl ether in the dog. *Lasers in Surgery and Medicine*, **18**(4): 406–409.

Pearce AI, Richards RG, Milz S, et al. 2007. Animal models for implant biomaterial research in bone: a review. *European Cells & Materials*, **13**: 1–10.

Pebam M, P SR, Gangopadhyay M, et al. 2022. *Terminalia chebula* polyphenol and near-infrared dye-loaded poly(lactic acid) nanoparticles for

imaging and photothermal therapy of cancer cells. *ACS Applied Bio Materials*, **5**(11): 5333–5346.

Pei SZ, Li HY, Chen LF, et al. 2024. Dual-functional AIE fluorescent probe for visualization of lipid droplets and photodynamic therapy of cancer. *Analytical Chemistry*, **96**(14): 5615–5624.

Peiffer Jr RL, Pohm-Thorsen L, Corcoran K. 1994. Models in ophthalmology and vision research. *In*: Manning PJ, Ringler DH, Newcomer CE. The Biology of the Laboratory Rabbit. Amsterdam: Elsevier, 409–433.

Peng CH, Li YS, Liang HJ, et al. 2011. Detection and photodynamic therapy of inflamed atherosclerotic plaques in the carotid artery of rabbits. *Journal of Photochemistry and Photobiology B: Biology*, **102**(1): 26–31.

Perry Y, Epperly MW, Fernando HC, et al. 2005. Photodynamic therapy induced esophageal stricture—an animal model: from mouse to pig. *Journal of Surgical Research*, **123**(1): 67–74.

Peyman GA, Kazi AA, Unal M, et al. 2000. Problems with and pitfalls of photodynamic therapy. *Ophthalmology*, **107**(1): 29–35.

Piksa M, Lian C, Samuel IC, et al. 2023. The role of the light source in antimicrobial photodynamic therapy. *Chemical Society Reviews*, **52**(5): 1697–1722.

Radu A, Conde R, Fontolliet C, et al. 2003. Mucosal ablation with photodynamic therapy in the esophagus: optimization of light dosimetry in the sheep model. *Gastrointestinal Endoscopy*, **57**(7): 897–905.

Radu A, Grosjean P, Jaquet Y, et al. 2005. Photodynamic therapy and endoscopic mucosal resection as minimally invasive approaches for the treatment of early esophageal tumors: pre-clinical and clinical experience in Lausanne. *Photodiagnosis and Photodynamic Therapy*, **2**(1): 35–44.

Rahn A, Drummelsmith J, Whitfield C. 1999. Conserved organization in the *cps* gene clusters for expression of *Escherichia coli* group 1 K antigens: relationship to the colanic acid biosynthesis locus and the *cps* genes from *Klebsiella pneumoniae*. *Journal of Bacteriology*, **181**(7): 2307–2313.

Ramos UD, Suaid FA, Wikesjö UME, et al. 2017. Comparison between two antimicrobial protocols with or without guided bone regeneration in the treatment of peri-implantitis. A histomorphometric study in dogs. *Clinical Oral Implants Research*, **28**(11): 1388–1395.

Reinke MH, Canakis C, Husain D, et al. 1999. Verteporfin photodynamic therapy retreatment of normal retina and choroid in the cynomolgus monkey. *Ophthalmology*, **106**(10): 1915–1923.

Reis TA, Jaculi AE, Ramos KLV, et al. 2019. Combination of cyclodextrin complexation and iontophoresis as a promising strategy for the cutaneous delivery of aluminum-chloride phthalocyanine in photodynamic therapy. *European Journal of Pharmaceutical Sciences*, **139**: 105056.

Ross HM, Smelstoys JA, Davis GJ, et al. 2006. Photodynamic therapy with motexafin lutetium for rectal cancer: a preclinical model in the dog. *Journal of Surgical Research*, **135**(2): 323–330.

Ross R. 1986. The pathogenesis of atherosclerosis--an update. *The New England Journal of Medicine*, **314**(8): 488–500.

Sakamoto FH, Tannous Z, Doukas AG, et al. 2009. Porphyrin distribution after topical aminolevulinic acid in a novel porcine model of sebaceous skin. *Lasers in Surgery and Medicine*, **41**(2): 154–160.

Salomao GHA, Fernandes AU, Baptista MS, et al. 2015. Chlorophyllin-M: a new substance for photodynamic therapy in the retina and choroid. *Lasers in Surgery and Medicine*, **47**(5): 421–425.

Sawa M, Awazu K, Takahashi T, et al. 2004. Application of femtosecond ultrashort pulse laser to photodynamic therapy mediated by indocyanine green. *British Journal of Ophthalmology*, **88**(6): 826–831.

Schlothauer JC, Hackbarth S, Jäger L, et al. 2012. Time-resolved singlet oxygen luminescence detection under photodynamic therapy relevant conditions: comparison of *ex vivo* application of two photosensitizer formulations. *Journal of Biomedical Optics*, **17**(11): 115005.

Segrest JP, Jones MK, De Loof H, et al. 2001. Structure of apolipoprotein B-100 in low density lipoproteins. *Journal of Lipid Research*, **42**(9): 1346–1367.

Sellera FP, Fernandes MR, Sabino CP, et al. 2019. Effective treatment and decolonization of a dog infected with carbapenemase (VIM–2)–producing *Pseudomonas aeruginosa* using probiotic and photodynamic therapies. *Veterinary Dermatology*, 2019, **30**(2): 170.

Sengupta P, Dutta S. 2020. Mapping the age of laboratory rabbit strains to human. *International Journal of Preventive Medicine*, **11**: 194.

Shafirstein G, Bellnier DA, Oakley E, et al. 2018. Irradiance controls photodynamic efficacy and tissue heating in experimental tumours: implication for interstitial PDT of locally advanced cancer. *British Journal of Cancer*, **119**(10): 1191–1199.

Shang Y, Zhang H, Cheng YJ, et al. 2022. Fluorescent imaging-guided chemo-and photodynamic therapy of hepatocellular carcinoma with HCPT@NMOFs–RGD nanocomposites. *International Journal of Nanomedicine*, **17**: 1381–1395.

She HC, Nakazawa T, Matsubara A, et al. 2007. Reduced photoreceptor damage after photodynamic therapy through blockade of nitric oxide synthase in a model of choroidal neovascularization. *Investigative Ophthalmology & Visual Science*, **48**(5): 2268–2277.

Shih MH, Huang FC. 2011. Effects of photodynamic therapy on rapidly growing nontuberculous mycobacteria keratitis. *Investigative Ophthalmology & Visual Science*, **52**(1): 223–229.

Sieber S, Grossen P, Detampel P, et al. 2017. Zebrafish as an early stage screening tool to study the systemic circulation of nanoparticulate drug delivery systems *in vivo*. *Journal of Controlled Release*, **264**: 180–191.

Siewerdsen JH, Moseley DJ, Burch S, et al. 2005. Volume CT with a flat-panel detector on a mobile, isocentric C-arm: pre-clinical investigation in guidance of minimally invasive surgery. *Medical Physics*, **32**(1): 241–254.

Sigusch B, Kranz S, Von Hohenberg AC, et al. 2023. Histological and histomorphometric evaluation of implanted photodynamic active biomaterials for periodontal bone regeneration in an animal study. *International Journal of Molecular Sciences*, **24**(7): 6200.

Sigusch BW, Pfitzner A, Albrecht V, et al. 2005. Efficacy of photodynamic therapy on inflammatory signs and two selected periodontopathogenic species in a beagle dog model. *Journal of Periodontology*, **76**(7): 1100–1105.

Silva Jr ZS, Bussadori SK, Fernandes KP, et al. 2015. Animal models for photodynamic therapy (PDT). *Bioscience Reports*, **35**(6): e00265.

Silva LO, Da Silva Souza KL, De Jesus Beloti L, et al. 2022. Use of photodynamic therapy and photobiomodulation as alternatives for microbial control on clinical and subclinical mastitis in sheep. *Lasers in Medical Science*, **37**(4): 2305–2310.

Singh D. 1993. Adaptive significance of female physical attractiveness: role of waist-to-hip ratio. *Journal of Personality and Social Psychology*, **65**(2): 293–307.

Spears JR, Serur J, Shropshire D, et al. 1983. Fluorescence of experimental atheromatous plaques with hematoporphyrin derivative. *The Journal of Clinical Investigation*, **71**(2): 395–399.

Srivastava PK, Han SS, Tu CC, et al. 2019. Phototoxicity generated by silicon quantum dot nanoparticles on zebrafish embryos. *ACS Applied Bio Materials*, **2**(7): 2872–2878.

Stoletov K, Klemke R. 2008. Catch of the day: zebrafish as a human cancer model. *Oncogene*, **27**(33): 4509–4520.

Su GY, Wei ZY, Wang LY, et al. 2020. Evaluation of toluidine blue-mediated photodynamic therapy for experimental bacterial keratitis in rabbits. *Translational Vision Science & Technology*, **9**(3): 13.

Sun L, Jiang WY, Zhang HR, et al. 2019. Photosensitizer-loaded multifunctional chitosan nanoparticles for simultaneous in situ imaging, highly efficient bacterial biofilm eradication, and tumor ablation. *ACS Applied Materials & Interfaces*, **11**(2): 2302–2316.

Sun MT, Cotton RM, Charoenkijkajorn C, et al. 2024. Evaluation of

verteporfin as a novel antifibrotic agent in a rabbit model of glaucoma filtration surgery: a pilot study. *Ophthalmology Science*, **4**(3): 100448.

Sunil V, Teoh JH, Mohan BC, et al. 2022. Bioengineered immunomodulatory organelle targeted nanozymes for photodynamic immunometabolic therapy. *Journal of Controlled Release*, **350**: 215–227.

Swartling J, Höglund OV, Hansson K, et al. 2016. Online dosimetry for temoporfin–mediated interstitial photodynamic therapy using the canine prostate as model. *Journal of Biomedical Optics*, **21**(2): 28002.

Tamaki Y. 2007. Novel approach for management of age-related macular degeneration--antiangiogenic therapy and retinal regenerative therapy. *Nippon Ganka Gakkai Zasshi*, **111**(3): 232–268.

Tawfik AA, Noaman I, El-Elsayyad H, et al. 2016. A study of the treatment of cutaneous fungal infection in animal model using photoactivated composite of methylene blue and gold nanoparticle. *Photodiagnosis and Photodynamic Therapy*, **15**: 59–69.

Tremblay A, Leroy S, Freitag L, et al. 2003. Endobronchial phototoxicity of WST 09 (Tookad), a new fast–acting photosensitizer for photodynamic therapy: preclinical study in the pig. *Photochemistry and Photobiology*, **78**(2): 124–130.

Tsilimbaris MK, Pallikaris IG, Naoumidi II, et al. 1994. Phthalocyanine mediated photodynamic thrombosis of experimental corneal neovascularization: effect of phthalocyanine dose and irradiation onset time on vascular occlusion rate. *Lasers in Surgery and Medicine*, **15**(1): 19–31.

Turubanova VD, Balalaeva IV, Mishchenko TA, et al. 2019. Immunogenic cell death induced by a new photodynamic therapy based on photosens and photodithazine. *Journal for Immunotherapy of Cancer*, **7**(1): 350.

Usui M, Asahara T, Naitoh Y, et al. 1999. Photodynamic therapy for the prevention of intimal hyperplasia in balloon–injured rabbit arteries. *Japanese Circulation Journal*, **63**(5): 387–393.

Van Staveren HJ, Bertrams RHP, Star WM. 1997. Bladder PDT with intravesical clear and light scattering media: effect of an eccentric isotropic light source on the light distribution. *Lasers in Surgery and Medicine*, **20**(3): 248–253.

Van Vugt DA, Krzemien A, Roy BN, et al. 2000. Photodynamic endometrial ablation in the nonhuman primate. *Journal of the Society for Gynecologic Investigation*, **7**(2): 125–130.

Visona A, Angelini A, Gobbo S, et al. 2000. Local photodynamic therapy with Zn(II)-phthalocyanine in an experimental model of intimal hyperplasia. *Journal of Photochemistry and Photobiology B: Biology*, **57**(2-3): 94–101.

Wachter E, Dees C, Harkins J, et al. 2003. Topical rose Bengal: pre-clinical evaluation of pharmacokinetics and safety. *Lasers in Surgery and Medicine*, **32**(2): 101–110.

Wang CJ, Qian Y. 2020. A water soluble carbazolyl-BODIPY photosensitizer with an orthogonal D–A structure for photodynamic therapy in living cells and zebrafish. *Biomaterials Science*, **8**(3): 830–836.

Wang LF, Qian Y. 2024. Heavy-atom-free BODIPY dendrimer: utilizing the spin–vibronic coupling mechanism for two-photon photodynamic therapy in zebrafish. *Journal of Materials Chemistry B*, **12**(25): 6175–6189.

Wang Q, Dong Y, Geng S, et al. 2014. Photodynamic therapy inhibits the formation of hypertrophic scars in rabbit ears by regulating metalloproteinases and tissue inhibitor of metalloproteinase–1. *Clinical and Experimental Dermatology*, **39**(2): 196–201.

Wang SW, Wu WB, Manghnani P, et al. 2019. Polymerization–enhanced two–photon photosensitization for precise photodynamic therapy. *ACS Nano*, **13**(3): 3095–3105.

Wang XB, Hu JM, Wang P, et al. 2015. Analysis of the *in vivo* and *in vitro* effects of photodynamic therapy on breast cancer by using a sensitizer, sinoporphyrin sodium. *Theranostics*, **5**(7): 772–786.

Wang XN, Luo D, Basilion JP. 2021. Photodynamic therapy: targeting cancer biomarkers for the treatment of cancers. *Cancers*, **13**(12): 2992.

Wasan KM, Cassidy SM. 1998. Role of plasma lipoproteins in modifying the biological activity of hydrophobic drugs. *Journal of Pharmaceutical Sciences*, **87**(4): 411–424.

Weersink RA, Forbes J, Bisland S, et al. 2005. Assessment of cutaneous photosensitivity of TOOKAD (WST09) in preclinical animal models and in patients. *Photochemistry and Photobiology*, **81**(1): 106–113.

Wei TT, Pan TZ, Peng XP, et al. 2024. Janus liposozyme for the modulation of redox and immune homeostasis in infected diabetic wounds. *Nature Nanotechnology*, **19**(8): 1178–1189.

Wilson CA, Saloupis P, Hatchell DL. 1991. Treatment of experimental preretinal neovascularization using photodynamic thrombosis. *Investigative Ophthalmology & Visual Science*, **32**(9): 2530–2535.

Xiao H, Liao Q, Cheng M, et al. 2009. 5-Amino-4-oxopentanoic acid photodynamic diagnosis guided microsurgery and photodynamic therapy on VX2 brain tumour implanted in a rabbit model. *Chinese Medical Journal*, **122**(11): 1316–1321.

Xiao ZW, Dickey D, Owen RJ, et al. 2007. Interstitial photodynamic therapy of the canine prostate using intra–arterial administration of photosensitizer and computerized pulsed light delivery. *Journal of Urology*, **178**(1): 308–313.

Yin W, Carballo-Jane E, Mclaren DG, et al. 2012. Plasma lipid profiling across species for the identification of optimal animal models of human dyslipidemia. *Journal of Lipid Research*, **53**(1): 51–65.

Yin XJ, Fang ZY, Fang Y, et al. 2022. Antimicrobial photodynamic therapy involving a novel photosensitizer combined with an antibiotic in the treatment of rabbit tibial osteomyelitis caused by drug–resistant bacteria. *Frontiers in Microbiology*, **13**: 876166.

Yoon I, Li JZ, Shim YK. 2013. Advance in photosensitizers and light delivery for photodynamic therapy. *Clinical Endoscopy*, **46**(1): 7–23.

Yu ZX, Meng XX, Zhang SN, et al. 2022. IR-808 loaded nanoethosomes for aggregation-enhanced synergistic transdermal photodynamic/photothermal treatment of hypertrophic scars. *Biomaterials Science*, **10**(1): 158–166.

Zhang F, Liu YM, Yang BS, et al. 2021. Tunable NIR AIE-active optical materials for lipid droplet imaging in typical model organisms and photodynamic therapy. *Journal of Materials Chemistry B*, **9**(10): 2417–2427.

Zhang Z, Liu Y, Chen YS, et al. 2019. Transdermal delivery of 5-aminolevulinic acid by nanoethosome gels for photodynamic therapy of hypertrophic scars. *ACS Applied Materials & Interfaces*, **11**(4): 3704–3714.

Zhou CC, Peng C, Shi CZ, et al. 2021. Mitochondria-specific aggregation-induced emission luminogens for selective photodynamic killing of fungi and efficacious treatment of keratitis. *ACS Nano*, **15**(7): 12129–12139.

Ziegler A, Gonzalez L, Blikslager A. 2016. Large animal models: the key to translational discovery in digestive disease research. *Cellular and Molecular Gastroenterology and Hepatology*, **2**(6): 716–724.